LUND UNIVERSITY

Thermoelectric Phenomena in Quantum Dots

Fahlvik Svensson, Sofia

2014

[Link to publication](#)

Total number of authors:
1

Thermoelectric Phenomena in Quantum Dots

Sofia Fahlvik Svensson

Doctoral Thesis
2014

LUND
UNIVERSITY

DOCTORAL THESIS
which, by due permission of the Faculty of Engineering, Lund University, Sweden,
will be defended in Rydbergsalen, Department of Physics, Sölvegatan 14, Lund,
Friday, October 17th, 2014 at 09:30.

Faculty opponent

Prof. Saskia Fischer

Humboldt-Universität zu Berlin

Organization:	Document name:
LUND UNIVERSITY	DOCTORAL DISSERTATION
Division of Solid State Physics Department of Physics, Box 118, S-221 00 Lund	Date of issue: 2014-09-22
Author: Sofia Fahlvik Svensson	Sponsoring organization

Title and subtitle: Thermoelectric phenomena in quantum dots

Abstract: Thermoelectricity is being intensively researched as it is believed to hold great promise for applications in power generation and cooling. One way to quantify the electrical power output of a thermoelectric material is the power factor, a function of electrical conductivity and thermopower. There are relationships between these relevant material properties that make efficient thermoelectric materials challenging to produce. The development of methods for creating nanostructured materials has allowed such trade-offs in material properties to be circumvented. Quantum dots are useful as model systems in this context since they have tunable energy filtering effects that are straightforward to characterize.

The work described in this thesis explores thermoelectric phenomena in quantum dots. The aim of this work was to gain a better understanding of the most basic thermoelectric behavior of quantum dots. This knowledge can provide deeper insight into which mechanisms may be of interest in increasing the efficiency of a thermoelectric material. A deeper understanding also allows the measurement method itself to be used as a tool for characterization. A thermoelectric measurement can complement the more commonly used electrical conductance measurements, by both confirming and supplementing data. This could be of great importance for the investigation of physical phenomena in nanostructures.

The quantum dots used in this work were defined in semiconductor nanowires. They were formed either by heterostructure growth or afterwards during fabrication of devices. The thermoelectric properties of the quantum dots were thoroughly investigated in the Coulomb blockade regime, and both linear and nonlinear responses as a function of the applied thermal gradient were observed and explained.

Thermoelectric measurements were also successfully used to characterize different InAs nanowire devices, either with the nanowire as is or covered by a polymer electrolyte. Closer investigations of these devices revealed physical properties of the nanowires that could be used to improve thermoelectric efficiency. In fact, this thesis presents the first measurements demonstrating an increase in thermoelectric power factor at low temperatures.

Key words: thermoelectric effect, quantum dot, nanowire, semiconductor

Classification system and/or index terms (if any)

Supplementary bibliographical information	Language: English

ISSN and key title	ISBN: 978-91-7623-064-0 (printed version) 978-91-7623-065-7 (electronic version)

Recipient's notes	Number of pages:	Price
	Security classification	

I, the undersigned, being the copyright owner of the abstract of the above-mentioned dissertation, hereby grant to all reference sources permission to publish and disseminate the abstract of the above-mentioned dissertation.

Signature: _____ Date: <u>2014-09-08</u>

Thermoelectric Phenomena in Quantum Dots

Sofia Fahlvik Svensson

Doctoral Thesis
2014

Front and back cover: Thermocurrent as a function of heating voltage and gate voltage obtained from an InAsP quantum dot defined in an InAs nanowire by InP barriers. The measurements were performed at a temperature of 13 mK, and the heating method developed in the present work was used to create the temperature gradient.

Contents

Abstract

Thermoelectricity is being intensively researched as it is believed to hold great promise for applications in power generation and cooling. One way to quantify the electrical power output of a thermoelectric material is the power factor, a function of electrical conductivity and thermopower. There are relationships between these relevant material properties that make efficient thermoelectric materials challenging to produce. The development of methods for creating nanostructured materials has allowed such trade-offs in material properties to be circumvented. Quantum dots are useful as model systems in this context since they have tunable energy filtering effects that are straightforward to characterize.

The work described in this thesis explores thermoelectric phenomena in quantum dots. The aim of this work was to gain a better understanding of the most basic thermoelectric behavior of quantum dots. This knowledge can provide deeper insight into which mechanisms may be of interest in increasing the efficiency of a thermoelectric material. A deeper understanding also allows the measurement method itself to be used as a tool for characterization. A thermoelectric measurement can complement the more commonly used electrical conductance measurements, by both confirming and supplementing data. This could be of great importance for the investigation of physical phenomena in nanostructures.

The quantum dots used in this work were defined in semiconductor nanowires. They were formed either by heterostructure growth or afterwards during fabrication of devices. The thermoelectric properties of the quantum dots were thoroughly investigated in the Coulomb blockade regime, and both linear and nonlinear responses as a function of the applied thermal gradient were observed and explained.

Thermoelectric measurements were also successfully used to characterize different InAs nanowire devices, either with the nanowire as is or covered by a polymer electrolyte. Closer investigations of these devices revealed physical properties of the nanowires that could be used to improve thermoelectric efficiency. In fact, this thesis presents the first measurements demonstrating an increase in thermoelectric power factor at low temperatures.

Populärvetenskaplig sammanfattning

Att en temperaturskillnad kan ge upphov till en elektrisk ström upptäcktes redan på 1800-talet och fenomenet är känt som den termoelektriska effekten. Denna effekt skulle kunna effektivisera energianvändningen överallt där det går att utnyttja en temperaturskillnad. Ett exempel är i en bil där en stor del av energin som tillförs genom bränsle förloras som spillvärme. Om denna spillvärme kunde användas för att driva ett termoelektriskt element istället för att bara slösas bort skulle bränsleförbrukningen kunna minskas. Under drygt tjugo år runt mitten av förra århundradet utvecklades, med hjälp av nyvunna kunskaper om halvledare, den teknologi som ännu idag används i många kommersiella termoelektriska element.

Dagens termoelement är inte särskilt effektiva och den termoelektriska effekten utnyttjas därför främst inom specialområden där storlek, hållbarhet och tillförlitlighet är viktigare än hur mycket energi som kan produceras. Ett exempel på ett sådant område är satelliter och rymdsonder där man använder radioisotopsgeneratorer. Dessa bygger på att termoelektriska element omvandlar den värme som produceras vid radioaktivt sönderfall till elektricitet.

Under 1990-talet förutspåddes utvecklingen inom nanoteknik vara lösningen för att förbättra effektiviteten hos termoelektriska material, och därmed göra dem gångbara som ett miljövänligt alternativ för att producera elektricitet, inte bara inom speciella applikationer, utan även i vårt dagliga liv. Med nanoteknik kan man producera material som består av komponenter som är mindre än 100 nanometer i åtminstone en dimension. Ett hårstrå är ungefär 70 000-100 000 nanometer tjockt. En sådan kraftig minskning av en komponents storlek gör att elektronerna inte längre kan röra sig i den riktningen, de begränsas alltså till rörelse i två dimensioner om den tredje dimensionen görs i nanoskala. Man kan begränsa elektronerna rörelsefrihet i ytterligare dimensioner genom att skala ner fler av komponentens sidor till nanostorlek, se Figur 1 för en illustrativ beskrivning av detta.

Förhoppningen är att man med hjälp av denna begränsning av elektronernas rörelsefrihet ska kunna kringgå ett fundamentalt problem med termoelektricitet:
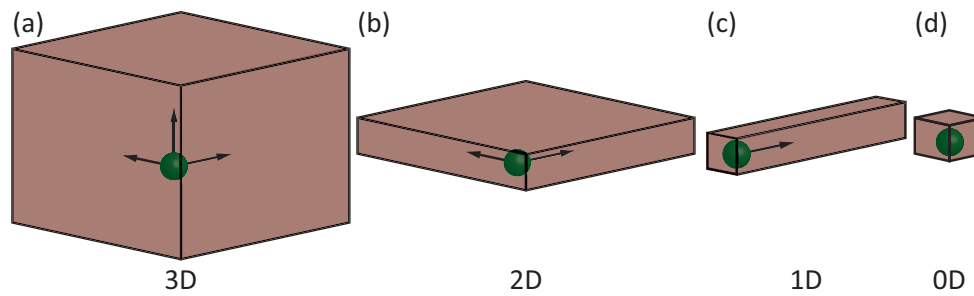
Figur 1. (a) Tredimensionell (3D) struktur. Pilarna indikerar att elektronen kan röra sig obehindrat i alla tre dimensioner. (b) Tvådimensionell (2D) struktur. Pilarna indikerar att elektronen enbart kan röra sig obehindrat i två dimensioner. (c) Endimensionell (1D) struktur. Elektronen kan enbart röra sig i en dimension. (d) Nolldimensionell (0D) struktur. Elektronen är förhindrad att röra sig i alla riktningar.

Ett effektivt termoelektriskt element måste ha tre egenskaper:

1. God elektrisk ledningsförmåga,

2. Dålig värmeledningsförmåga,

3. En liten temperaturskillnad bör ge upphov till en stor spänning, eller med andra ord; hög termoelektrisk effekt.

Dessa tre egenskaper är mer eller mindre omöjliga att kombinera i tredimensionella (3D) material, till exempel medför en god elektrisk ledningsförmåga också en god värmeledningsförmåga. I nanostrukturer gäller dock inte längre de samband mellan ovanstående egenskaper som omöjliggör ett effektivt termoelektriskt element. Man har redan bevisat att man i en endimensionell (1D) struktur, en nanotråd (Figur 2), kan minska värmeledningsförmågan med hjälp av de reducerade dimensionerna utan att påverka övriga egenskaper hos materialet.

Vår forskning fokuserar på en struktur som förhindrar elektronernas rörelse i alla riktningar – en nolldimensionell kvantprick (Figur 1 (d)) i en nanotråd (Figur 2). Det speciella med en sådan kvantprick är att man kontrollerat kan tillåta elektroner att passera genom den och att man också kan välja vid vilken energi detta sker. Vi vill försöka förstå de mest grundläggande termoelektriska fenomen som uppstår när man utsätter en kvantprick för en temperaturskillnad. Denna information kan i framtiden ligga till grund för utvecklingen av effektivare termoelektriska material. Som bonus har vi insett att termoelektriska mätningar i sig själva kan användas för att komplettera strömmätningar när man undersöker låg-dimensionella system, något som tidigare inte har utnyttjats i särskilt stor utsträckning.
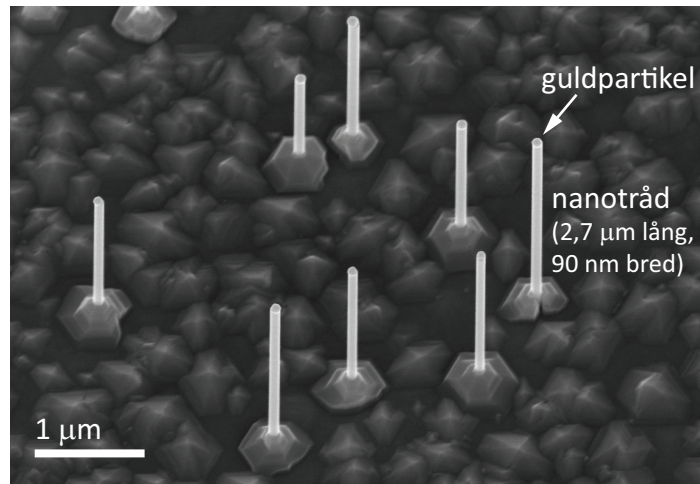
Figur 2. Nanotrådar växta från guldpartiklar på en InAs yta. Partiklarna har placerats ut med hjälp av en slumpmässig process, och nanotrådarna växer där partiklarna placerats.

Ett oväntat resultat av vår forskning är att vi har kunnat se en ökning i termoelektrisk effektivitet i 1D nanotrådar vid temperaturer nära den absoluta nollpunkten (-270 to -250 °C). Det är första gången någon har observerat en sådan ökning. Denna ökning är nära knuten till kvantprickar. Det har visat sig att svagt definierade kvantprickar i nanotrådar är nyckeln till en ökad termoelektrisk effekt i vårt fall. Detta är ett mycket lovande resultat eftersom det möjliggör användning av tjockare nanotrådar, vilka är lättare att tillverka. Sannolikt är det möjligt att utnyttja effekten i många parallellkopplade nanotrådar, vilket är en förutsättning för att kunna använda nanotrådarna i kommersiella sammanhang.

Abbreviations

CBE	Chemical Beam Epitaxy
DOS	Density Of States
EBL	Electron Beam Lithography
LHe	Liquid Helium
MBE	Molecular Beam Epitaxy
MOVPE	Metal-Organic Vapor Phase Epitaxy
SEM	Scanning Electron Microscopy
TEM	Transmission Electron Microscopy
2DEG	Two Dimensional Electron Gas

Symbols

a	Lattice constant
C	Capacitance
E	Energy
e	Electron charge (1.60219×10^{-19} C)
$f(E)$	Fermi-Dirac distribution
G	Electrical conductance
h	Planck's constant (6.62607×10^{-34} Js)
I	Current
I_H	Heating current
I_{th}	Thermocurrent
k	Boltzmann constant (1.38065×10^{-23} J/K)
P_H	Heating power
R	Resistance
S	Thermopower (Seebeck coefficient)
T	Temperature
V	Voltage
V_g	Gate voltage
V_H	Heating voltage
V_{th}	Thermovoltage
Γ	Full width at half maximum
μ	Electrochemical potential
σ	Electrical conductivity
τ	Transmission function

List of publications

This thesis is based on the following papers, which will be referred to in the text by their Roman numerals.

I. Control and understanding of kink formation in InAs–InP heterostructure nanowires

S Fahlvik Svensson, S Jeppesen, C Thelander, L Samuelson, H Linke and K A Dick
Nanotechnology **24**, 345601 (2013)

I participated in planning the experiments, performed all the material growth and performed all the characterization and analysis with the exception of the transmission electron microscopy. I also mainly responsible for writing of the paper.

II. Fully tunable, non-invasive thermal biasing of gated nanostructures suitable for low-temperature studies

J G Gluschke, S Fahlvik Svensson, C Thelander and H Linke
Nanotechnology **25**, 385704 (2014)

Claes Thelander and I conceived the device design. I grew the nanowires and contributed to the interpretation of the data and writing of the paper.

III. Lineshape of the thermopower of quantum dots

S Fahlvik Svensson, A I Persson, E A Hoffmann, N Nakpathomkun, H A Nilsson, H Q Xu, L Samuelson and H Linke
New Journal of Physics **14**, 033041 (2012)

I performed parts of the modeling and participated in writing the paper.

IV. Nonlinear thermovoltage and thermocurrent in quantum dots

<u>S Fahlvik Svensson</u>, E A Hoffmann, N Nakpathomkun, P M Wu, H Q Xu, H A Nilsson, D Sánchez, V Kashcheyevs and H Linke
New Journal of Physics **15**, 105011 (2013)

I fabricated some of the devices and performed some of the measurements. I was mainly responsible for the data analysis and the writing of the paper.

V. Large thermoelectric power factor enhancement observed in InAs nanowires

P M Wu, J Gooth, X Zianni, <u>S Fahlvik Svensson</u>, J G Gluschke, K A Dick, C Thelander, K Nielsch and H Linke
Nano Lett. **13**, 4080-4086 (2013)

I grew the nanowires, fabricated some of the devices and performed some of the measurements. I participated in the data analysis and in writing the paper.

VI. Using polymer electrolyte gates to set-and-freeze threshold voltage and local potential in nanowire-based devices and thermoelectrics

<u>S Fahlvik Svensson</u>, A M Burke, D J Carrad, M Leijnse, H Linke and A P Micolich
Submitted

I planned the project and designed the experiment together with colleagues at The University of New South Wales, Australia. I grew the nanowires, performed most of the experimental measurements, and was mainly responsible for the data analysis and the writing of the paper.

The following paper is relevant, but not included in this thesis:

Conductance enhancement of InAs/InP heterostructure nanowires by surface functionalization with oligo-phenylenevinylenes

M I Schukfeh, K Storm, A Mahmoud, R R Søndergaard, A Szwajca, A Hansen, P Hinze, T Weimann, <u>S Fahlvik Svensson</u>, A Bora, K A Dick, C Thelander, F C Krebs P Lugli, L Samuelson and M Tornow
ACS Nano **7**, 4111–4118 (2013)

1. Introduction

Fossil fuels have enabled the industrial development of the Western world. However, the world's energy consumption is increasing every year, and our primary sources of energy are being depleted. Furthermore, environmental concerns, such as pollution and global warming, are associated with the use of fossil fuels. In an attempt to amend this situation, considerable effort has been devoted to finding alternative forms of energy based on renewable sources such as sunlight, wind, waves, etc. The main objective is to develop methods that are affordable and efficient enough to sustain our need for energy.

The thermoelectric effect is a physical phenomenon currently attracting considerable interest. It is the phenomenon by which a voltage difference is created by a temperature gradient across a sample (Figure 1.1 (a)). The amplitude of the voltage produced is material specific, and the relationship between the temperature gradient and the induced voltage is referred to as either the Seebeck coefficient or thermopower. This effect could be used to harvest energy by converting waste heat into electric power. One can imagine it applied in a car, where more than half of the supplied fuel energy is lost as heat. The thermoelectric effect can also be employed in reverse; i.e., a temperature difference can be induced across a sample by applying a voltage (Figure 1.1 (b)). The thermoelectric effect can therefore also be used for cooling applications, such as domestic refrigeration.

Although the thermoelectric effect was discovered in 1823, it took more than a hundred years before it attracted any real interest from the research community. By then, semiconductors had been discovered, and Abram Ioffe showed that doped semiconductors far exceeded previously tested materials in thermoelectric efficiency [1]. This revelation led to an intense search for the most efficient thermoelectric material available, and almost all semiconductors, semimetals and alloys known at the time were investigated. In fact, the field of semiconductor research was driven, for a number of years, not by micro- and optoelectronics, but by the prospect of efficient refrigeration [2].
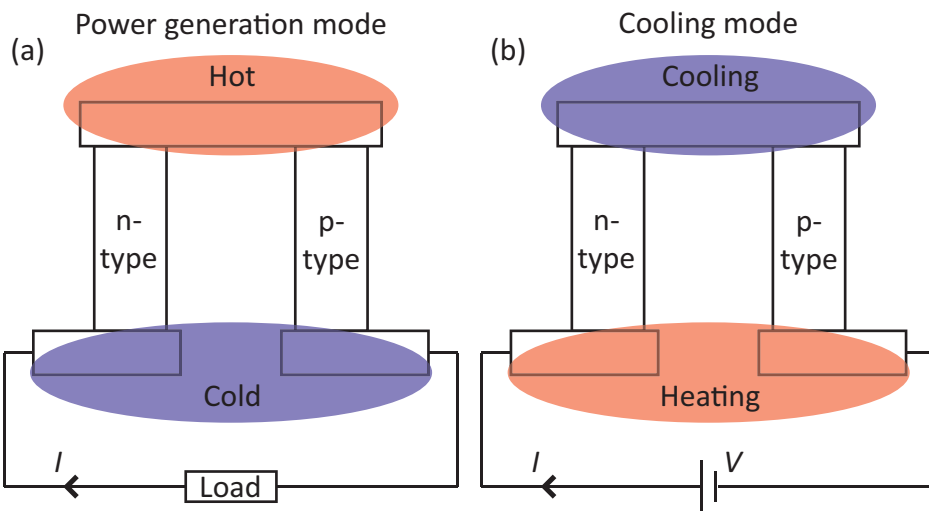
Figure 1.1. (a) A thermoelectric element consisting of an n-type and a p-type semiconductor connected in series. The applied temperature difference creates a current that can be used to extract useful work. (b) The same thermoelectric element as in (a), but now a current flows through the circuit as a result of the applied voltage, and a temperature difference arises between the two ends of the element.

Initial research in the 1950s failed to result in a thermoelectric material that could compete in efficiency with compressor-based refrigerators. The three properties of a material that influence its thermoelectric efficiency: electrical conductivity, thermal conductivity, and thermopower, were simply too interdependent to allow for further advances. The ratio of the electronic contribution to the thermal conductivity and the electrical conductivity of metals is, for example, proportional to the temperature according to the Wiedemann-Franz law [3], and the thermopower and the electrical conductivity are related via the location of the Fermi level in the band gap. Therefore, the use of the thermoelectric effect was limited to special applications where reliability and convenience outweighed cost [2, 4].

However, interest in the field was renewed at the beginning of the 1990s. New methods of fabricating nanostructured materials showed promise in circumventing the limiting relationships mentioned above, which were making efficient thermoelectric materials impossible [2, 4]. Research on thermoelectrics in different nanostructured materials has been conducted for over twenty years. Two major themes can be identified: the reduction of thermal conductivity, and the improvement of the so-called power factor, i.e., the product of electrical conductivity and the square of the thermopower, which describes the electric power output.

Efforts to reduce thermal conductivity in materials have been rather successful, leading to an increase in the thermoelectric efficiency [5]. The main concept employed is to increase phonon scattering, thereby reducing the lattice thermal

14

conductivity [6]. However, improving the power factor has proved to be more difficult. The aim is basically to use nanostructuring to distort the electronic density of states (DOS) of a material, and thereby increase the power factor. According to theory, the power factor should increase monotonically with decreasing size of a two-dimensional (2D) or one-dimensional (1D) system [7, 8]. The optimal thermoelectric material would have a DOS consisting of a delta function [9], and a zero-dimensional (0D) structure would have a DOS consisting of a series of delta functions. Such a structure could rely on energy-filtering mechanisms which, at least theoretically, would make it possible to reach Carnot efficiency [10]. Figure 1.2 shows the DOS for systems of different dimensions.
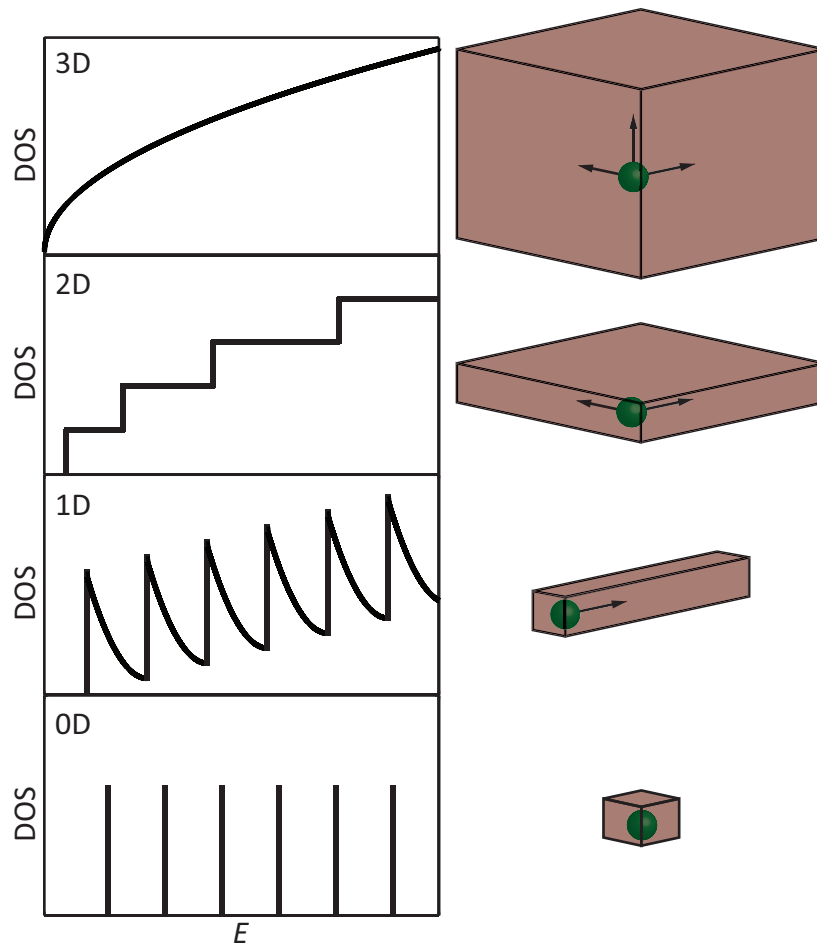

Figure 1.2. Density of states (DOS) as a function of energy, E, for three-dimensional (3D), two-dimensional (2D), one-dimensional (1D) and zero-dimensional (0D) systems.

This thesis describes thermoelectric measurements on 0D structures; i.e., quantum dots in semiconductor nanowires. The main objective was to gain a thorough understanding of the basic mechanisms behind the thermoelectric response of such a device, rather than investigating the thermoelectric efficiency. The concept of thermal conductance, which is dominated by phonons in a semiconductor, is therefore not explicitly discussed in this work. There are two main reasons why a thorough understanding of the thermoelectric response is important. Firstly, if the basic mechanisms can be explained and understood, they could be exploited to develop efficient thermoelectric materials, and secondly, the thermoelectric response has so far been an underused tool in device characterization, despite the fact that it has many interesting aspects that could be utilized.

To form the quantum dots used in the present work semiconductor heterostructure nanowires were grown epitaxially, by seeding with Au particles. A problem that can occur during such heterostructure growth, when switching from say InAs to InP, is that the nanowire changes growth direction. It was in this work concluded that such incidents can be suppressed by increasing the amount of In supplied during growth.

A temperature gradient was needed for the thermoelectric measurements. If the measurements are performed at low temperatures, as in the present work, it is important to realize this temperature gradient without increasing the surrounding temperature. As no existing techniques were satisfactory for our purposes a new heater design was developed, a technique that allows for efficient formation of a temperature gradient along the length of the nanowire without much affect on the surrounding temperature.

The thermoelectric response of the quantum dots was thoroughly investigated in the Coulomb blockade regime. It has in the literature been difficult to find agreement between modeling and measurements, but it was in the present work shown that the lineshape of the thermovoltage can be understood if different energy scales of the transmission function are taken into consideration. The lineshape can also be predicted by a Landauer-type model if these energy-dependent parameters are extracted from the electrical conductance measurements.

As the applied thermal gradient was increased in our measurements highly nonlinear behavior was observed in the thermoelectric response of the quantum dots. Such nonlinear behavior has been observed for quantum dots previously in the literature, but it has never been explained. By performing 2D scans as a function of heating voltage and gate voltage a movement of the energy levels of the quantum dot with respect to the gate voltage was detected as the applied thermal bias was increased. This renormalization of the quantum dot energy levels was shown to explain the highly nonlinear behavior seen in the thermoelectric measurements.

16

InAs nanowires without deliberately defined quantum dots were studied with thermoelectric measurements. An increase in power factor was seen at low temperatures, but could not be explained by the more traditional theories about power factor enhancement in 1D systems. The increase was instead attributed to interference effects between propagating states and quantum dot-like states in the nanowires. These measurements were the first measurements demonstrating an increase in thermoelectric power factor in nanowires.

Measurements were also performed on InAs nanowires covered by a polymer electrolyte. The effect of this polymer electrolyte on the nanowire was studied at low temperatures, where the polymer electrolyte 'freezes' in the sense that the ionic mobility drops to zero. It was shown that the polymer electrolyte could be used to create a fixed charge environment for the nanowire, and that quantum dot-like behavior could be induced. The compatibility between this polymer electrolyte and thermoelectric measurements was also confirmed.A brief summary of the chapters of this thesis follows:

Chapter 2 provides an introduction to thermoelectric behaviour of low-dimensional structures, specifically quantum dots. Chapters 3 and 4 describe the growth of nanowires and quantum dots and the fabrication of devices. The experimental setup is presented in Chapter 5 and the theoretical framwork for quantum dots in Chapter 6. Chapter 7 presents thorough investigations of the thermoelectric behavior of quantum dots in the linear and the nonlinear regime with respect to the applied thermal gradient. The usefulness of thermoelectric measurements as a characterization tool is described in Chapter 8 and the thesis is summarized in Chapter 9.

2. Thermoelectricity

In 1821, Thomas Johann Seebeck observed that a temperature difference across a junction of two dissimilar metals produced a voltage, or an electric current if the circuit was closed. This phenomenon would later come to be known as the thermoelectric effect [11]. A few years later, in 1834, Jean Charles Athanase Peltier discovered that the effect also worked in reverse, and demonstrated that an electric current could be used to produce a temperature difference [12].

In the 1950s semiconductors and their newly found transport properties were introduced into the world of thermoelectricity [1]. The mechanisms discovered during this period are still broadly used in today's thermoelectric elements. The thermoelectric effect is attractive in its simplicity. The possibility of generating electrical power from a difference in temperature would be convenient in many situations. However, as a result of poor efficiency it has so far been limited to niche applications, such as space missions, where reliability, durability and size are more important than efficiency [2, 4].

It was predicted that developments in nanotechnology in the 1990s would lead to important advances in the efficiency of thermoelectric materials [2, 4]. It has also been theoretically predicted that a 0D object, i.e., a quantum dot, could reach Carnot efficiency, when used as a heat engine, due to its energy filtering effects [10, 13]. However, it has proven difficult to confirm these exceptional theoretical predictions, and the significant breakthroughs that will make thermoelectrics commercially viable have yet to be made.

A brief introduction to thermoelectricity and its most basic principles is given in the following sections.

2.1   Current driven by temperature difference

The total current through a material, when both a voltage V and a temperature difference ΔT are applied, can in linear response be described as:

$$I_{tot} = GV + G_S\Delta T, \tag{1}$$

where G is the electrical conductance of the material and G_S is the transport coefficient which relates ΔT to current. If no current is allowed to flow through the material ($I_{tot} = 0$, open-circuit conditions) the thermovoltage, V_{th}, is the voltage V that is needed to counteract the current created by ΔT,

$$V_{th} = -\frac{G_S}{G}\Delta T = S\Delta T, \tag{2}$$

where $S = -G_S/G$ is the thermopower. By convention, S is negative for n-type materials and positive for p-type materials.

The current arising from the application of a temperature difference can be explained by considering electron transport through a three-dimensional (3D) n-type material, as shown in Figure 2.1. The electrons in the hot reservoir on the left have a greater spread in energy due to the higher temperature on this side, and as the density of states shown in Figure 2.1 indicates, states above the electrochemical potential, μ, are available for transport in the 3D material. Electrons with high energy can therefore traverse the material from the hot reservoir on the left to the cold reservoir on the right where states are also available. In the same way, electrons below μ can move
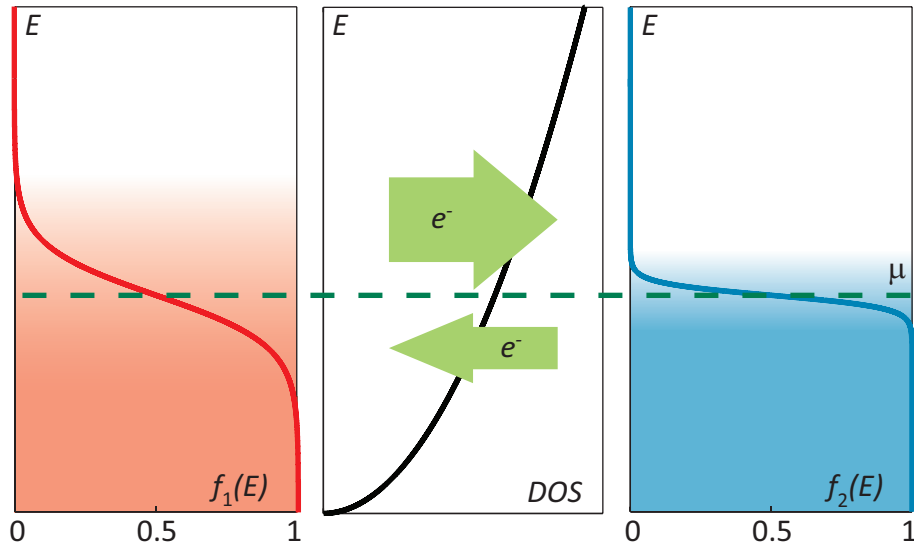
Figure 2.1. A 3D material, in the center, with the characteristic square-root increase in DOS (black line) as a function of energy, E, is connected to a hot reservoir on the left and a cold reservoir on the right. The temperature difference is illustrated by the two differently smeared Fermi-Dirac distributions, $f_1(E)$ and $f_2(E)$, on either side of the 3D material. No voltage bias is applied so the electrochemical potential, μ, shown by the dashed green line, is the same throughout the device.

20

from the cold reservoir on the right to the hot reservoir on the left, as states are available in both the 3D material and in the hot reservoir on the left. States are available under the electrochemical potential on the hot side since the electrons that have gained more energy due to the higher temperature have left vacant states behind. A net current is created because the 3D material has more available states above μ than below, which leads to a net flow of electrons from the left (hot side) to the right (cold side). If the temperature gradient is applied under open-circuit conditions, where no net current is allowed to flow through the material, the voltage that arises to counteract the net flow of electrons is the thermovoltage.

The simple illustration in Figure 2.1 indicates that thermoelectric measurements contain a great deal of information that can be used for diagnostics. For example, information about charge carriers can be obtained by simply applying a temperature difference across a material. If the material in Figure 2.1 had been p-type instead, the resulting net current would have flowed in the opposite direction, since the DOS would have decreased as a function of energy, instead of increased. This information could not have been deduced by applying a voltage to the material and measuring the resulting current.

2.2   Going to fewer dimensions

The shape of the DOS of a material governs its thermoelectric properties, as indicated by the example in Figure 2.1. One way of influencing the DOS of a material is to reduce the number of dimensions by nanostructuring [4]. It has been theoretically predicted that reducing the dimensionality of a material to two [8], one [7] or zero dimensions [10] will improve the thermoelectric efficiency. In fact, the ideal DOS for maximizing the efficiency of a thermoelectric material has been shown to be a delta function [9].

Consider a DOS consisting of a delta function between a hot and a cold contact, similar to the setup for the 3D material illustrated in Figure 2.1. Because of the DOS chosen, there is only one energy, E_0, at which electrons can be transported across the material. Let us now see what happens in such a structure when a temperature difference is applied, in the same manner as in Figure 2.1. Since the left side has a higher temperature than the right side, the peak in DOS can be positioned so that electrons have enough energy to cross from left to right (hot to cold), but not from right to left (cold to hot), as illustrated in Figure 2.2. If this is done under open-circuit conditions ($I = 0$), the electrons will start piling up on the right since they cannot escape that contact. As a result of this accumulation of electrons, the
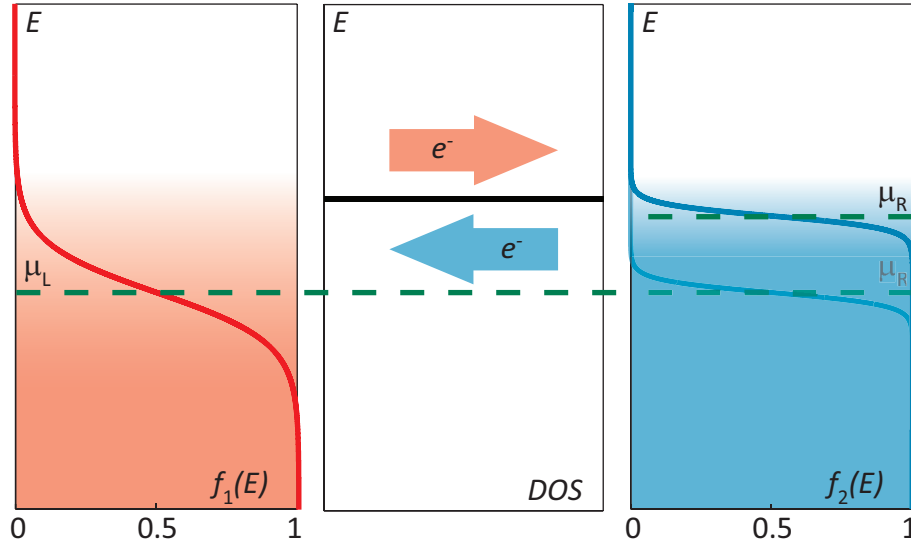
Figure 2.2. A material (center) with a DOS consisting of a delta function located at energy E_0 (black line) is connected to a hot reservoir on the left and a cold reservoir on the right. The temperature difference is illustrated by the two differently smeared Fermi-Dirac distributions, $f_1(E)$ and $f_2(E)$, on either side of the structure. To maintain the open-circuit condition ($I = 0$) the electrochemical potential on the right, μ_R, must increase compared to the electrochemical potential on the left, μ_L, to counteract the flow of electrons from left to right due to the applied temperature difference.

electrochemical potential of the right (cold) contact will start to rise, and will continue to increase until the two Fermi-Dirac functions on either side of the structure are equal ($f_1(E, \mu_L, T_L) = f_2(E, \mu_R, T_R)$), which is the only condition under which the current can be maintained at zero in this kind of setup. The thermovoltage can then be regarded as the difference in electrochemical potential between the left (hot) and the right (cold) side, induced by the applied temperature gradient.

The energy, E_0, at which the delta function is positioned can be chosen so that there is no change in the entropy of the system [10]. This means that electrons can be exchanged reversibly between the left and the right side in Figure 2.2. This makes it possible to construct a heat engine using such a structure, which could, in principle, operate at Carnot efficiency [10]. There are no materials available with a DOS consisting of a single delta function, but it is possible to achieve one that gets fairly close. A 0D structure ideally has a DOS consisting of a series of delta peaks. A quantum dot has a DOS consisting of peaks, although they have a finite width.

Quantum dots can be physically defined in several ways. The most common within electron transport physics studies is to define the quantum dot electrostatically in a two-dimensional electron gas (2DEG). A 2DEG is a structure in which the electrons
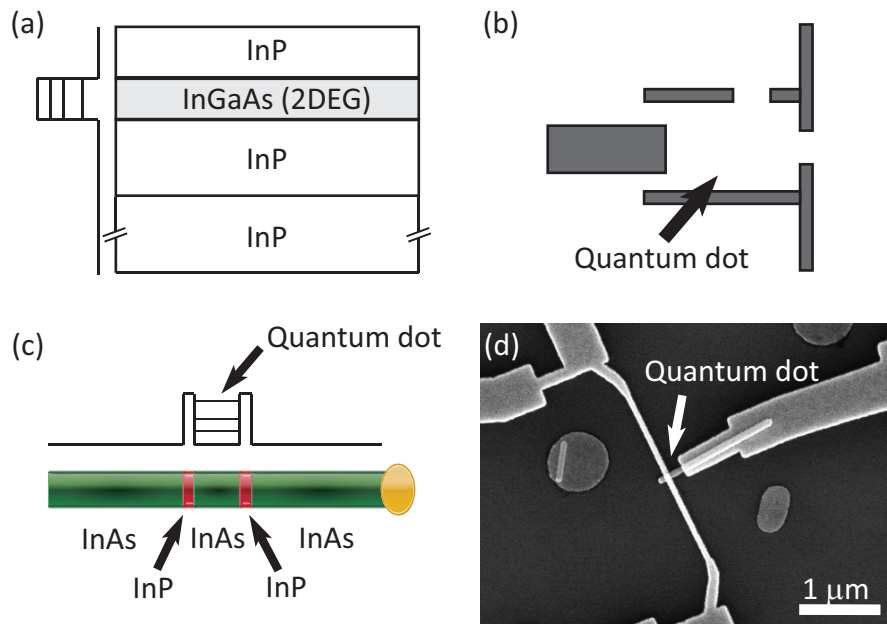
Figure 2.3. (a) Schematic illustration of a possible combination of materials to create a 2DEG with a corresponding sketch of the conduction band energy on the left. (b) A possible pattern of gate electrodes defining a quantum dot in a 2DEG based on the pattern used by Staring et al [14]. (c) A quantum dot defined in a heterostructure semiconductor nanowire consisting of InAs and InP segments. The yellow colored ellipse symbolizes the Au particle used to seed the nanowire growth. A sketch of the conduction band energy is shown above the nanowire. (d) A quantum dot formed in an InSb nanowire by Schottky barriers introduced through the contacts, which were also used for transport measurements.

are confined in one dimension and allowed to move freely in the other two (Figure 2.3 (a)) [15, 16]. The quantum dot is defined by a pattern of gates on top of the structure, and the gates are used to deplete the 2DEG below, as shown in Figure 2.3 (b). Another approach is based on defining the quantum dot in a 1D semiconductor nanowire, as shown in Figure 2.3 (c) and (d) [17, 18]. A quantum dot grown in a nanowire has the advantage of very sharp interfaces between the different materials, resulting in a very well-defined quantum dot, however, there is a loss in flexibility and tuning possibilities compared to a quantum dot defined in a 2DEG. It is the nanowire-based approach that has been used in the work described in this thesis.

3. Nanowires

A semiconductor nanowire is a rod-shaped structure that normally has a diameter of less than 100 nm and a length of a few μm [19, 20]. The high aspect ratio of nanowires ideally allows the confinement of electrons in two of the three dimensions, implying that they are 1D objects [21, 22]. However, it is preferable to consider nanowires as quasi-1D systems with respect to electron transport as they have a certain cross-sectional area. A quantum dot can be defined in a nanowire either during the growth of the nanowire or afterwards, during the contacting procedure. Both methods have been employed in the studies presented in this thesis to measure thermoelectric effects on quantum dots. When defined during growth, this was done by changing the growth precursors for short periods of time, alternating between materials with a smaller and a larger bandgap [23]. When the quantum dot was defined during the contacting procedure, the potential barriers forming the quantum dot were introduced through Schottky contacts [18]. All nanowires were grown epitaxially, seeded by gold (Au) particles. A brief introduction to nanowire growth from Au particles and its most basic mechanisms is given in this chapter. Most of the nanowires were grown using chemical beam epitaxy (CBE), a method that will also be described here. The indium antimonide (InSb) nanowires described in Paper IV (with quantum dots defined by electrical contacts), were grown by metal-organic vapor phase epitaxy (MOVPE). For information about this growth method see, for example, Ref. [24]. CBE is not the most common technique used for nanowire growth today, but it has some some features making it suitable for the growth of quantum dots; for example, sharp interfaces can be obtained when switching from indium arsenide (InAs) to indium phosphide (InP). However, one problem associated with this technique is that the nanowires tend to kink at the InP–InAs interface if the growth conditions are not optimized. This is discussed in Section 3.3 and Paper I.

3.1 Nanowire growth

A substrate with Au particles deposited on it is placed in a growth chamber. The Au particles can be deposited by different techniques; in this work aerosol-deposited [20] or electron beam lithography (EBL)-defined particles [25] were used. The substrate
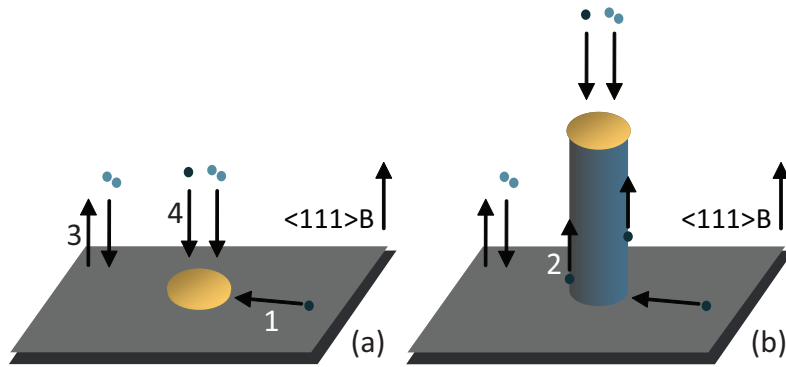
Figure 3.1. Schematic illustration of InAs nanowire growth. A gold particle is deposited on an InAs (111)B substrate. The sample is then mounted in the CBE equipment. After adjusting the temperature, the growth precursors (trimethyl indium (TMIn) and tertiarybutyl arsine (TBAs)) are introduced into the growth chamber. It is more energetically favorable for growth to take place underneath the Au particles, so the supply of material results in nanowire growth. See Section 3.2 for an explanation of the arrows marked 1-4.

usually consists of the same material as the nanowires to be grown. Precursors containing the growth materials are supplied to the growth chamber, for example In and As for InAs nanowires. If the correct conditions are applied, e.g., temperature and material supply rate, the Au particles function as catalysts for nanowire growth. There will be competing growth on the surrounding substrate surface as well as on the nanowire side facets, but the growth rate in these regions is normally much lower than the growth rate of the nanowires under the Au particles. As more and more material is supplied, the Au particles are elevated by the crystal growth underneath, and nanowires are formed. For a schematic illustration see Figure 3.1. The Au particles are not consumed during growth, and the completed nanowire will therefore still have a Au particle at the top.

The diameter and density of the resulting nanowires are governed by the size and density of the original Au particles, whereas the length of the nanowire can be controlled by the amount of growth material supplied and the growth temperature.

3.2   Chemical beam epitaxy

Chemical beam epitaxy, sometimes also referred to as metal-organic molecular beam epitaxy, is a growth technique that combines the metal-organic sources from MOVPE with the beam technology associated with molecular beam epitaxy (MBE) [26]. The growth process takes place in a high-vacuum growth chamber, as in MBE, with a background pressure of less than 10^{-7} mbar. To maintain a high vacuum during

growth, several vacuum pumps are incorporated into the growth system, as well as a cryogenic shroud using liquid nitrogen, where gas in the system can condense to improve the pumping efficiency. This results in a pressure of 10^{-5} to 10^{-4} mbar in the growth chamber during growth. A schematic illustration of the CBE equipment is given in Figure 3.2.

The precursors used in CBE are, as most often in MOVPE, metal-organic molecules. In the CBE system used in this work the molecule sources are stored in their liquid phase in overpressured bottles that are kept in a water bath at a constant temperature of 10 °C. During growth the molecules are injected into the growth chamber as a beam which impinges onto the heated growth substrate (also referred to as the sample) at an incident angle of 8° with respect to the normal of the surface. Growth then takes place through chemical reactions at the substrate surface.

Trimethyl indium (TMIn) was used as the group-III precursor to grow nanowires. The TMIn decomposes at the substrate surface, where it dissociates into its alkyl

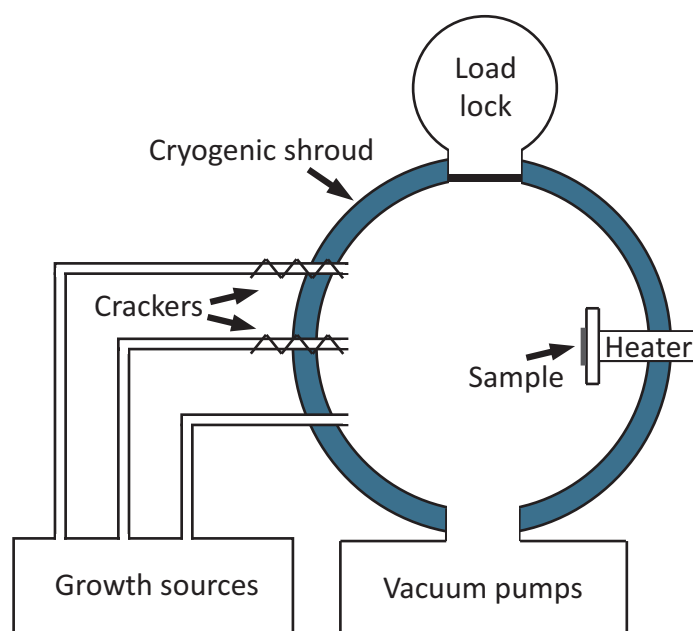**Figure 3.2**. Schematic illustration of the high-vacuum growth chamber of the CBE equipment used to grow nanowires in this work. The sample is positioned on a heater that supplies heat to achieve the desired growth temperature. The surrounding cryogenic shroud helps the vacuum pumps maintain a sufficiently low pressure during growth. In order not to disrupt the vacuum, samples are inserted and removed through a load lock.

radicals and eventually elemental In atoms [27]. These In atoms can then be incorporated into the nanowire. Two different group-V precursors were used: tertiarybutyl arsine (TBAs) and tertiarybutyl phosphine (TBP). Both group-V precursors are thermally cracked at 1100 °C as they enter the growth chamber. This cracking process results in As_2, As_4, AsH_3 and C_4H_8 in the case of TBAs, and P_2, PH_3 and C_4H_8 for TBP [28]. The two different decomposition mechanisms for the group-III and group-V molecules result in different behavior regarding the incorporation of atoms during growth. The group-III precursor diffuses on the growth substrate and on the nanowire side facets (as illustrated by arrows 1 and 2 in Figure 3.1), and nanowire growth therefore relies on an available surface collection area for In, which will depend on the density of the nanowires, and the growth temperature, etc. [29, 30]. The group-V precursors, on the other hand, can only contribute to nanowire growth when impinging directly on the seed particle since they have negligible migration lengths on the growth substrate (as shown by arrows 3 and 4 in Figure 3.1) [27].

The use of metal-organics in CBE has as consequence that carbon can be incorporated into the crystal during growth. Carbon atoms act as donors in InAs nanowires [31], and this together with band bending at the InAs surface [32] results in the InAs nanowires being n-type.

3.3   Heterostructure nanowires

One of the most interesting characteristics of nanowires is their capability to accommodate strain [33]. Materials with different lattice constants, a, such as InAs ($a = 6.058$ Å at 300 K) and InP ($a = 5.869$ Å at 300 K), can therefore be grown on top of each other without disturbing the crystallinity of the nanowire. Combining layers of material in a nanowire in this manner is referred to as axial heterostructure growth, and it can be used to create quantum dots in nanowires, as in this work.

Figure 3.3 shows a schematic illustration of the process of growing an InAs quantum dot defined by InP barriers in an InAs nanowire. The procedure starts with the growth of an InAs nanowire on an InAs (111)B substrate, as shown in Figure 3.1. When the length of the first InAs segment is sufficient, the group-V precursor is switched from TBAs to TBP and InP is grown instead (Figure 3.3 (a)). In the work described in this thesis it is important that the InAs segment is sufficiently long to accommodate an electrical contact, and these parts of the nanowire are referred to as leads, as shown in Figure 3.3 (d). When an InP barrier of the appropriate length has been grown, the group-V precursor is switched back to TBAs for the growth of InAs
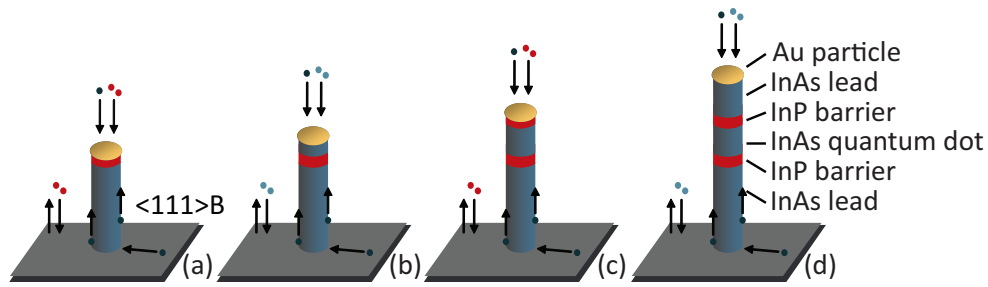
28

Figure 3.3. Schematic illustration of the growth of an axial quantum dot defined by InP barriers in an InAs nanowire. (a) An InAs nanowire has been grown, as shown in Figure 3.1, and the group-V precursor has been switched to TBP to grow an InP barrier on top of the InAs. (b) The group-V precursor is switched back to TBAs so that InAs grows again. This segment will be the actual quantum dot. (c) InP is grown on top of the InAs quantum dot segment to form the other barrier. (d) Finally, the group-V precursor is switched back to TBAs to complete the growth of the heterostructure nanowire.

(Figure 3.3 (b)). The length of the InP barrier depends on the required strength of the coupling between the InAs quantum dot and the InAs lead, and is normally 2-8 nm. When the InAs quantum dot has the required length, the group-V precursor is switched again to TBP for growth of the second InP barrier (Figure 3.3 (c)). The nanowire is then capped off with a second InAs lead by switching the group-V precursor once more to TBAs, to make room for an electrical contact on this side of the quantum dot as well (Figure 3.3 (d)). Figure 3.4 (a) - (b) shows transmission electron microscopy (TEM) images of an InAs quantum dot defined by InP barriers in an InAs nanowire.

Although nanowires are appropriate for heterostructure growth, some complications can arise, namely grading and kinking. Grading is the gradual change from one material to the other, instead of a sharp interface between the two [34-36]. This problem was not encountered in the CBE system used for the growth of nanowires in the present work. (See Figure 3.4 (a) - (c) for examples of interfaces between InP and InAs grown in the CBE.) Kinking occurs when the nanowire changes direction during growth [37-39]. This, on the other hand, was a problem when growing heterostructures with CBE, as discussed in Paper I. An example of a kinked nanowire among straight nanowires can be seen in Figure 3.4 (d). Kinking was found to occur only at the interface between InP and InAs, and only when grown in that particular sequence (Paper I). The probability of kinking was found to be highly dependent on the amount of available In in the system, and could be completely suppressed by adjusting the growth conditions.
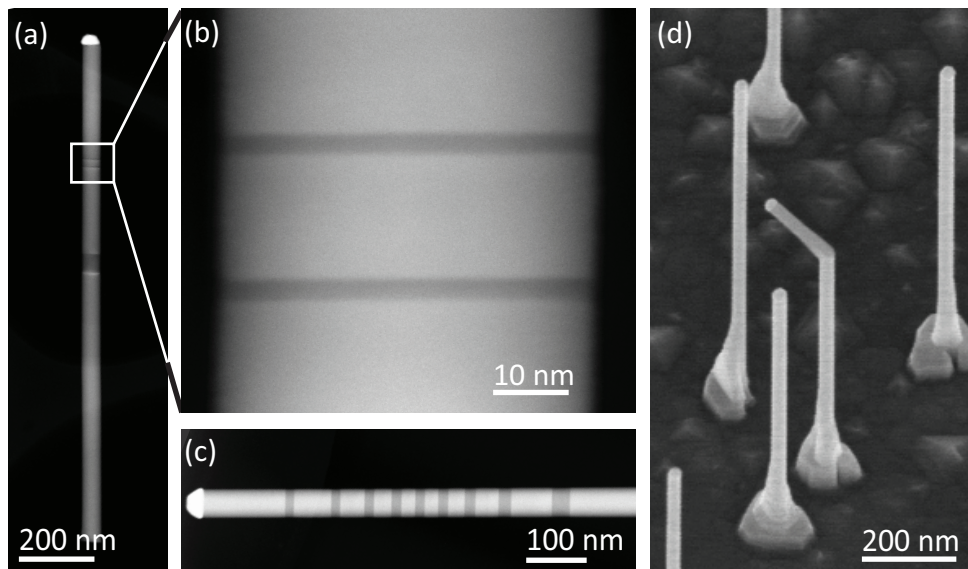
Figure 3.4. (a) High angle annular dark field scanning transmission electron microscopy (HAADF-STEM) image of an InAs nanowire (bright contrast) with InP barriers (darker contrast) forming an InAs quantum dot. The thicker InP segment halfway up the nanowire is introduced to stabilize the InP growth rate, to simplify the growth of two evenly long InP barriers for the quantum dot. (b) A HAADF-STEM image showing an enlargement of the region in (a), focusing on the quantum dot. (c) A HAADF-STEM image showing that it is possible to switch back and forth between InAs and InP many times once the right growth conditions have been established. (d) Scanning electron microscopy (SEM) image of axially heterostructured InAs-InP nanowires grown with CBE. Some nanowires grow straight under these growth conditions, whereas others kink when switching from InP to InAs. Dr. Sebastian Lehmann is gratefully acknowledged for the TEM imaging.

30

4. Device fabrication

The electric characterization of a nanowire requires electrical contacts. To be able to perform thermoelectric measurements on a nanowire there is also a need for a heater to create the required temperature gradient. This chapter describes how contacts were made to nanowires in this work, and how the heaters were designed and fabricated.

4.1   Contacting a nanowire

The process of making contacts to a nanowire begins by transferring the nanowires from the growth substrate onto a piece of Si wafer covered with a 110 nm layer of SiO_2. This chip has a predefined pattern of Au bond pads and markers to simplify the contacting process, as shown in Figure 4.1 (a). The preparation of these pre-patterned pieces of Si/SiO_2 is explained in Appendix A. In the work presented in this thesis nanowires were transferred to the chip using a piece of cleanroom tissue. In the case of the chips shown in Figure 4.1 (a) the nanowires were deposited in the middle of
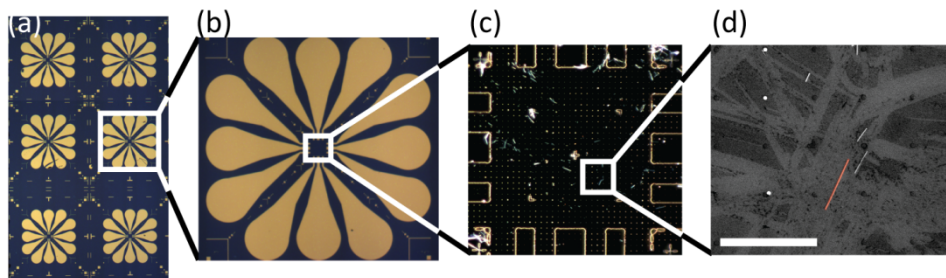
Figure 4.1. (a) Bright-field optical microscopy image of a Si/SiO_2 chip used to make contacts to nanowires, showing the pre-defined markers and bond pads. The size of the chip is 3 x 5 mm. (b) Bright-field optical microscopy image of one of the flower-like structures on the Si/SiO_2 chip showing the 12 bond pads. The size of each flower is 1 x 1 mm. The nanowires are deposited in the middle of each "flower". The size of the area inside the bond pads is 70 x 70 μm. (c) Dark-field optical microscopy image of the center of a flower-like structure with deposited nanowires. (d) SEM image of some of the nanowires deposited in (c). The nanowire highlighted in red would typically be a good choice for making a device. The scale bar is 5 μm.

what looks like a flower with 12 petals (Figure 4.1 (b)). There are six such "flowers" on each chip, each with twelve bond pads. The transfer process is repeated until there are at least two nanowires sufficiently separated in each flower-like structure to make contacts to both of them. This is checked using dark field imaging in an optical microscope. An example of the successful transfer of nanowires is shown in Figure 4.1 (c) and (d). After the transfer process, images of the positions of the nanowires are obtained either with the optical microscope used during the nanowire transfer (Figure 4.1 (c)), or using scanning electron microscopy (SEM) (Figure 4.1 (d)). When the nanowire positions have been determined the pattern of the electrical contacts to the nanowires can be drawn. This can either be done semi-automatically in a LabVIEW program used to identify the positions of the nanowires, or the contacts can be drawn from scratch using the Raith 150 EBL software.

A resist is then spun onto the chip (Figure 4.2 (a) - (b)) and EBL is used to define the contact pattern (Figure 4.2 (c)). Before evaporation of the contact metals (a sticking layer of either Ni or Ti followed by Au was used for all devices discussed in this thesis, Figure 4.2 (d)) and subsequent lift-off (Figure 4.2 (e)), the nanowire surface is prepared for electrical contacts by sulfur passivation. The purpose of this step is to remove the surface oxide, without etching away too much of the nanowire material, and to simultaneously passivate the nanowire surface with covalently bonded sulfur atoms [40, 41]. After lift-off, during which the resist is dissolved and the excess metal removed, the sample is ready for measurements. For more details on the fabrication process, see Appendix B.

(a) Nanowire deposited on substrate

(b) Coating with resist

(c) Electron beam lithography

(d) Deposition of contact metal

(e) Lift-off
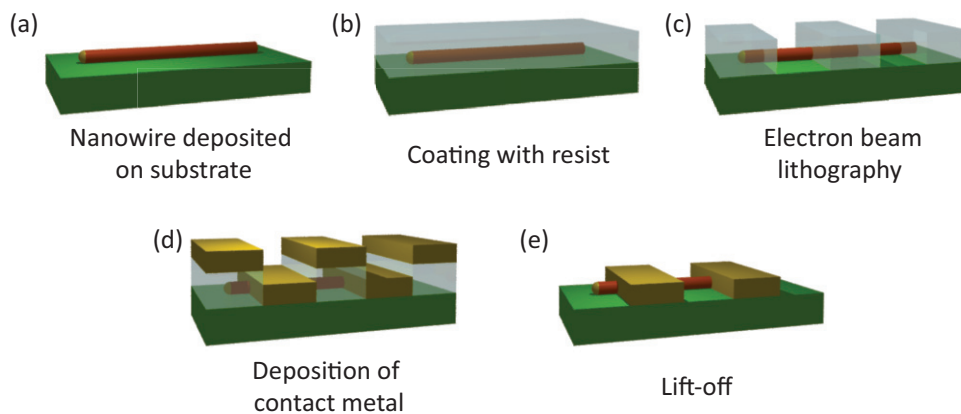
Figure 4.2. Schematic illustration of the process of making electrical contacts to a nanowire. (a) Nanowires are deposited on the Si/SiO$_2$ substrate. (b) A resist is spun onto the substrate. (c) EBL is used to make a pattern in the resist. (d) The contact metal is deposited onto the sample by evaporation. (e) Lift-off is performed to remove the remaining resist, and at the same time all excess metal is removed. Only the desired contacts remain.

4.2   Heater design and fabrication

A temperature difference must be generated along the length of the nanowire to allow thermoelectric measurements. This was achieved in the present work using ohmic heating of metal strips. Various designs were used, as described below.

4.2.1   Contact heating

One method of inducing a temperature gradient is to heat the electron gas directly at one end of the nanowire by using the ohmic contact to the nanowire also as a heater, see Figure 4.3 (a). This method has the advantage of requiring no extra processing steps when making contacts to the nanowire since the contact and the heater are one and the same. If experiments are performed at low temperatures there is no need to rely on electron-phonon coupling for heat transfer to create the temperature gradient, since the electrons are heated directly via ohmic heating. However, this method is somewhat cumbersome, i.e., the heating voltages must be fine-tuned so that they do not result in overall biasing of the nanowire, which would interfere with the measurements [42, 43]. Figure 4.3 (a) shows the circuitry needed to apply a temperature gradient using this heating method. For the same reason, it is inconvenient to change the amount of heating since the device must be recalibrated for each new heating voltage.

4.2.2   Side heating

Another option for creating a temperature difference is to place the heater strip just next to one end of the nanowire, as shown in Figure 4.3 (b). This design also requires only one EBL step during processing, and has the advantage of separating the heater from the actual contact to the nanowire, which simplifies measurements. No balancing of voltages is needed, and it is possible to tune the heating voltage independently of the measurement circuit. The disadvantage is that the heat must be transferred from the heater strip to the electron gas in the contact via the substrate. This is a rather inefficient way of creating a temperature gradient across the sample, and will lead to heating of the contact furthest away [44-46], which is supposed to remain at its original temperature. In fact, to create a temperature gradient of 0.1 K per micrometer along the nanowire a heating power, P_H, of several mW may be needed. This can result in an overall increase in the surrounding temperature of 5-10 times that of the temperature difference created [44, 45]. Such large values of P_H can cause a noticeable increase in the temperature of the sample space of a low-
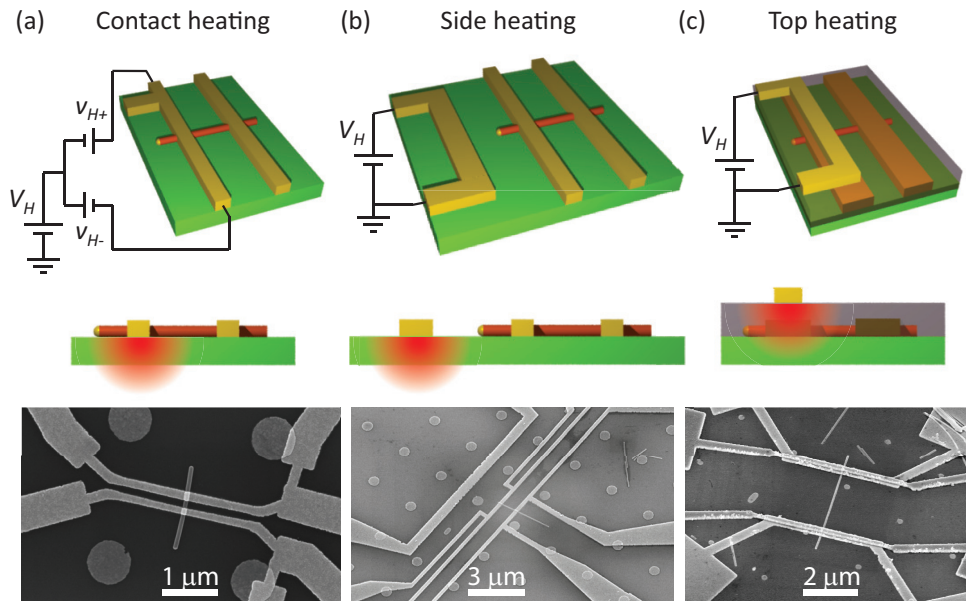
Figure 4.3. Schematic illustrations of three different heater designs: a) contact heating, b) side heating, and c) top heating. The images below are SEM micrographs of the corresponding designs.

temperature refrigerator [44]. This complicates comparisons of conductance measurements made without a temperature gradient and thermoelectric measurements, since it is difficult to distinguish between the effects of the applied temperature gradient and the effects of the increase in overall temperature. In the worst case, it can even make low-temperature measurements impossible [44].

4.2.3 Top heating

The most efficient method of applying a temperature gradient was a new heater design developed in this work, and described in Paper II. The idea is basically to place the heater strip on top of the contact to the nanowire, and electrically separate the heater and the contact by a thin layer of oxide, as illustrated in Figure 4.3 (c). In this study a 10 nm layer of HfO_2 was used as the insulating layer. The advantage of this design is that the heater is much closer to the nanowire than would be possible if the heater was defined in the same EBL step as the contacts, as is the case with the side-heating design. The disadvantage is that device fabrication is more complicated. After fabrication of the device, as described in Section 4.1, the sample must be cleaned in an oxygen plasma ashing system before it is transferred to an atomic layer deposition system for the deposition of 10 nm of HfO_2 covering the entire chip. Holes are thereafter made in the oxide using a SEM equipped with a focused ion beam to allow

for electrical contact between the heater and the bond pads on the chip. Once the holes have been created, the sample is coated with resist and baked, and EBL is then used to define the pattern of the heater on top of the oxide. The pattern is thereafter developed, and the device is cleaned in an oxygen plasma ashing system, after which layers of Ni (5 nm) and Au (100 nm) are evaporated onto the sample. After the lift-off process, the sample is ready for measurements.

As demonstrated in Paper II, this method of heating is a significantly more efficient way to create a temperature gradient than placing the heater strip next to the nanowire. It creates very large temperature gradients at small heating powers: $\Delta T = 17.4$ K at $T = 50$ K for $P_H = 0.88$ mW, and $\Delta T = 37.6$ K at $T = 295$ K for $P_H = 5.3$ mW. Furthermore, the other end of the nanowire is not heated as much as in previously presented techniques. No increase was seen in the temperature of the other end of the nanowire at 50 K, and only a 2 K increase was seen at 295 K using the heating powers mentioned above. The design still has a separate circuit for heating, as does the side-heating technique, which simplifies measurements considerably compared to the case when the heater and the electrical contact to the nanowire are combined, as in the contact-heating technique.

5. Experimental setup

To be able to measure the properties of low-dimensional systems, the thermal energy kT must be smaller than the other energy scales of the system, e.g. the charging energy of a quantum dot (defined in Chapter 6). This was accomplished throughout the studies presented in this thesis with help of different kinds of low-temperature refrigerators. The basic principles behind such refrigerators are described in this chapter. The electric signals measured at these low temperatures in a low-dimensional system are typically small. The voltage bias applied is usually smaller than kT. Different techniques can be employed to obtain an optimized signal-to-noise ratio. A summary of the measurement techniques used is therefore presented. This chapter also briefly explains different thermometry techniques that can be utilized to determine the applied temperature gradient in thermoelectric experiments.

5.1   Low-temperature refrigerators

There are various ways of achieving low temperatures, but the techniques used in this thesis all involve liquids of different kinds with very low boiling points. Various systems are illustrated in Figure 5.1, and will be described below. The simplest method used (Paper II) was to immerse the sample in liquid helium (LHe) at a temperature of 4.2 K (Figure 5.1 (a)). The temperature of the sample can be increased by withdrawing the sample out of the liquid into the He atmosphere above it. The temperature can be controlled by varying the distance between the sample and the liquid surface.

To reach temperatures below 4.2 K ($kT \approx 0.36$ meV) the vapor pressure of LHe can be reduced by pumping on the vapor above the LHe bath with a vacuum pump. The atoms in the vapor phase that are removed will be replaced by atoms leaving the surface of the liquid. These atoms have the most energy, and therefore the liquid will cool due to the decrease in average energy. This phenomenon is known as evaporative cooling. It is possible to reach temperatures below 1 K by pumping on a LHe bath [47]. The region where pumping occurs is therefore often referred to as the 1K pot; see Figure 5.1 (b). Temperatures of around 1.7 K ($kT \approx 0.15$ meV) were achieved
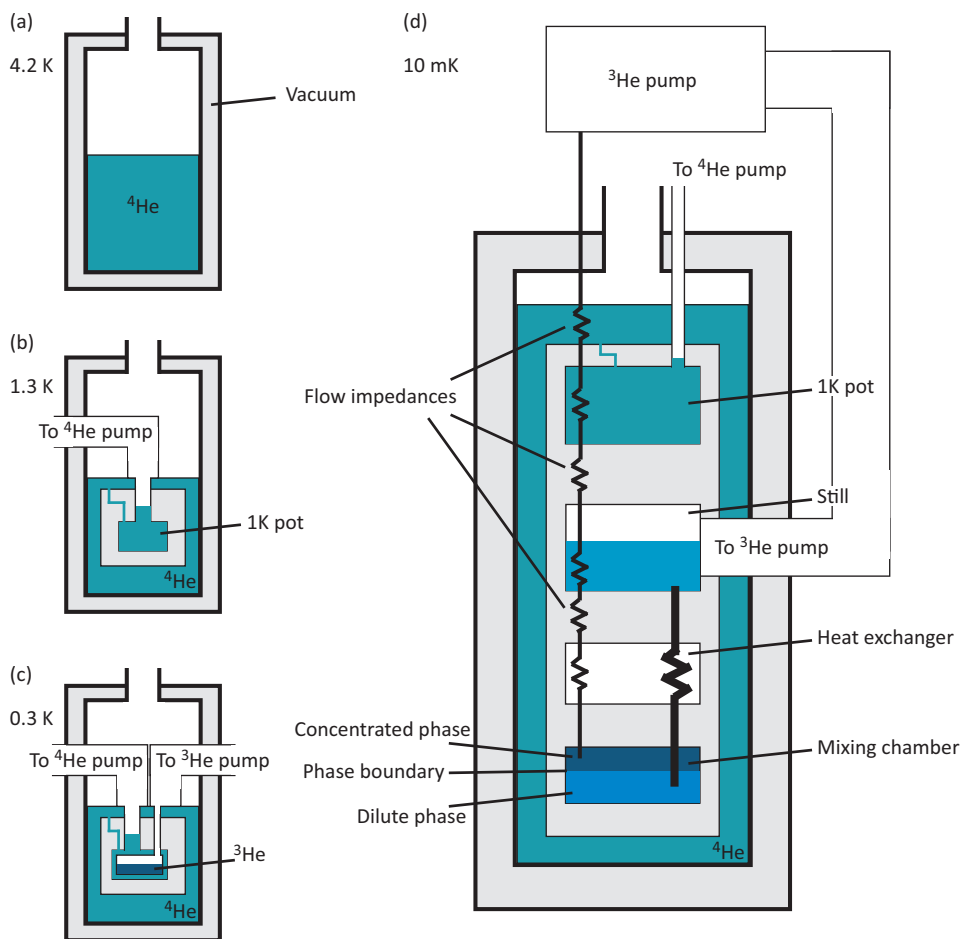
Figure 5.1. (a) Schematic illustration of the LHe dewar used for measurements at 4.2 K. (b) Schematic illustration of the ^{4}He refrigerator with its 1K pot, which makes it possible to reach a temperature of 1.3 K. (c) Schematic illustration of the ^{3}He cryostat with the ^{3}He bath used to reach a temperature of 300 mK. (d) Schematic illustration of the dilution refrigerator with the mixing chamber, where the processes of transferring ^{3}He gas between the different phases of the ^{3}He/^{4}He mixture results in extremely low temperatures of about 10 mK.

using the variable temperature Janis system available at the Division of Solid State Physics. It is also possible to heat the sample space to reach temperatures up to 200 K, which makes it a very appealing system for temperature-dependent measurements, and was therefore a very suitable system for the measurements described in Paper V.

To achieve temperatures below 1.3 K (the temperature normally accessible by pumping on He) different isotopes of He must be utilized. There are two stable He isotopes, ^{3}He and ^{4}He [47]. ^{4}He is the more common isotope, previously referred to in this chapter as helium. To reach stable temperatures below 1.3 K the much rarer

38

isotope ^{3}He must be used. When the vapor pressure of liquid ^{3}He is reduced, in the same manner as for ^{4}He, temperatures down to 0.3 K ($kT \approx 26\mu$eV) can be achieved [47]. In cryostats using this technique ^{4}He is first pumped to reach 1.3 K. ^{3}He gas is then led into the space where it liquefies. Once the ^{3}He is in its liquid form it is pumped on to reach 0.3 K (Figure 5.1 (c)). When all the liquid has been evaporated, the ^{3}He is recondensed so that the process can be repeated [47]. ^{3}He cryostats therefore have a limited time during which they can remain at this low temperature. The hold time of a ^{3}He refrigerator must therefore be taken into account when performing measurements. It should also be mentioned that ^{3}He is a rare isotope, and therefore very expensive (on average 140 times more expensive than ^{4}He in 2010). Refrigerators of this type were used to obtain the measurements presented in Papers IV and VI.

To reach temperatures even lower than 0.3 K, a dilution refrigerator can be used, which relies on mixing of ^{3}He and ^{4}He in a mixing chamber. Cooling in such a system occurs when ^{3}He atoms are transferred from the ^{3}He-rich liquid (the concentrated phase) to the ^{4}He-rich liquid (the dilute phase). The basic principles of this refrigeration technique are illustrated in Figure 5.1 (d), and will be explained briefly below. For a more extensive explanation see Refs. [47, 48]. A bath of liquid ^{4}He is used to cool the incoming ^{3}He gas to 4.2 K. The ^{3}He gas is then condensed by a pumped ^{4}He environment (as described above), which usually results in temperatures of around 1.2-1.5 K. The now liquid ^{3}He is then led through a still (see Figure 5.1 (d)), which has a temperature of around 0.7 K. On its way to the still and as it flows further down into the system the liquid is passed through flow impedances to prevent it from re-evaporating. The liquid is thereafter passed through heat exchangers to reach a temperature as close as possible to that of the mixing chamber, before it finally enters the mixing chamber. The actual cooling takes place in the mixing chamber. The ^{3}He-rich liquid has a lower density and will therefore float on top of the ^{4}He-rich liquid. The ^{3}He gas entering the mixing chamber will thus reach the concentrated phase first, then pass the phase boundary and enter the dilute phase. The cooling power of the system is determined by the amount of heat needed to dilute the ^{3}He as it passes the phase boundary [47, 48]. The dilute phase then leaves the mixing chamber and is driven back up to the still by the continuous pumping on the still, which reduces the concentration of ^{3}He. (Pumping also reduces the temperature of the still to about 0.7 K.) Osmosis is the mechanism driving the ^{3}He from the dilute phase up to the still to restore the equilibrium concentration. This, in turn, disturbs the equilibrium concentration in the dilute phase and ^{3}He atoms therefore move from the concentrated phase to the dilute phase, which results in cooling [47]. As the ^{3}He liquid moves from the mixing chamber to the still it passes the heat exchangers, cooling the warmer liquid that is on its way down to the mixing

39

chamber. He is evaporated in the still (mainly ^{3}He since it has a higher vapor pressure than ^{4}He at this temperature), and can be removed by a pump at room temperature. The extracted gas is then returned to the system to be cooled once more by the ^{4}He bath. Performing this process in a closed circuit provides a method of continuous cooling to very low temperatures. Commercial dilution refrigerators today normally reach around 10 mK ($kT \approx 0.86\mu eV$), but temperatures down to 2 mK are possible [47].

Due to the rapid increase in the price of liquid ^{4}He, and the fact that it does not exist in abundance on Earth, cryogen-free dilution refrigerators are rapidly becoming more popular. The name is, however, somewhat misleading since the system requires the same mixture of ^{3}He and ^{4}He as a standard dilution unit. However, the ^{4}He bath used to pre-cool the ^{3}He gas is not needed, as pre-cooling is achieved by pulse tubes which rely on cooling by compression of a working gas (normally He) [48]. The basic idea of cooling via pulse tubes is explained below, and a more thorough description can be found in Ref. [48].

In a pulse tube, a compressor periodically varies the pressure of the working gas via a moving piston. The pulse tube is thermally isolated from its surroundings and has heat exchangers at both ends, one hot and one cold, as shown in Figure 5.2. The hot heat exchanger is connected to a buffer via a flow resistance. Gas flows to the pulse tube from the buffer if the pressure of the pulse tube, p_{pt}, is lower than the pressure of the buffer, p_b, ($p_{pt} < p_b$). If instead $p_{pt} > p_b$, the gas will flow back through the hot heat exchanger and into the buffer. Since the pulse tube is thermally isolated, the gas leaving the pulse tube will have a higher temperature than when it entered from
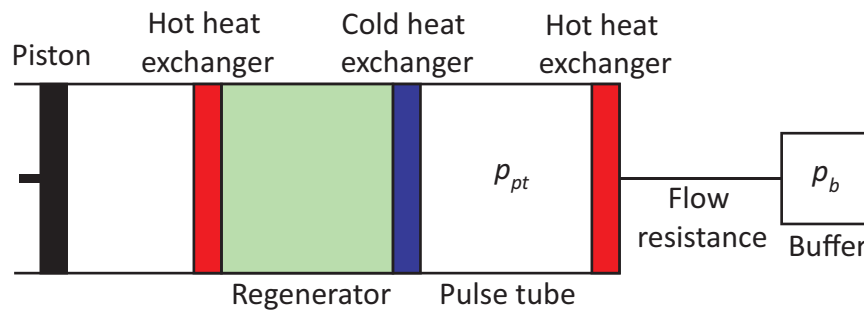
Figure 5.2. Schematic illustration of a pulse tube refrigerator. The piston compresses the working gas, thereby regulating the pressure of the pulse tube, p_{pt}. Depending on whether p_{pt} is higher or lower than the pressure of the buffer (p_b) the gas will either move to the right or the left. Gas flowing through the regenerator will either give off or take up heat from the regenerator material, depending on the direction in which it is flowing.

the buffer. Heat can therefore be released from the hot heat exchanger to its surroundings. A similar process, but opposite, takes place at the cold heat exchanger at the other end of the pulse tube. Gas enters the pulse tube after having passed through the regenerator when p_{pt} is high. As the gas passes through the regenerator from left to right it gives off heat to the regenerator material. It will therefore have a lower temperature when it passes through the cold heat exchanger to the right of the regenerator compared to what it had at the heat exchanger to the left. When the pressure is reduced and the gas returns through the cold heat exchanger on its way back from the pulse tube it will have an even lower temperature than when it entered. Due to the lower temperature of the gas flowing back through the cold heat exchanger cooling takes place here.

A cryogen-free Triton dilution refrigerator from Oxford Instruments was installed at the Division of Solid State Physics in 2013, with which a temperature of 12.3 mK ($kT \approx 1.06\mu\text{eV}$) can be achieved.

5.2   Measurement setup

The same basic procedure is followed to measure on a sample, regardless of the cooling method used. The chip containing the devices (with contacted nanowires) is mounted on a chip carrier using an electrically conducting glue, as shown in Figure 5.3 (a). The legs of this chip carrier are then connected to the bond pads on the chip using a wire bonding machine (Figure 5.3 (b)), so that the device can be accessed electrically with macroscopic measurement equipment. The devices are thereafter
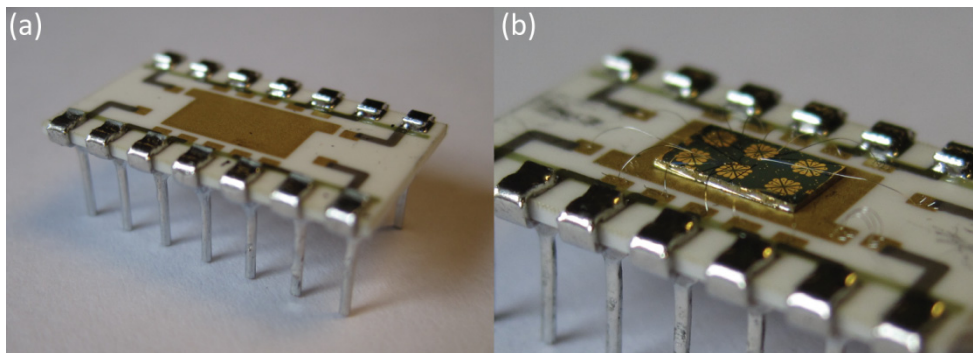

Figure 5.3. (a) Photograph of a chip carrier onto which chips with nanowire devices can be glued so that electrical contact can be made with macroscopic equipment. (b) A chip carrier with a chip glued onto it. Looking closely, it is possible to see the bonding wires that connect the bond pads on the chip to the legs of the chip carrier.

checked for electrical functionality at room temperature, using voltage sources, current amplifiers, and multimeters. A promising device normally has a resistance of around 10 kΩ if it is a homogeneous InAs nanowire, and between 100 kΩ to tens of MΩ depending on the specific structure if it is a heterostructure nanowire. The functionality of the back gate should also be tested. This is done by applying a voltage to the back gate and simultaneously monitoring the current flowing through the nanowire. When electrically promising nanowire devices have been identified, the chip is cooled down.

Once it has been cooled, the nanowire device can be thoroughly investigated. Characterization of a device normally starts with measurements of its conductance, for example, as illustrated in Figure 5.4 (a). Different measurement techniques can be employed; both AC and DC measurements have been performed in this work. AC measurements have the advantage of usually having a lower signal-to-noise ratio since lock-in techniques can be used [49]. It is important to remember that AC measurements are differential, as the change in current due to the change in the applied voltage is measured. The ratio between the small current measured and the applied voltage is therefore a good approximation of dI/dV if the applied AC voltage is small (much smaller than kT).

To measure the thermoelectric response, a temperature gradient must be applied. This can be done with both AC and DC techniques depending on the heating method used (a DC measurement setup is shown in Figure 5.4 (b)). If measurements of the AC thermoelectric response are performed, the lock-in must be set to 2nd harmonic measurements. This can be understood if the resulting increase in
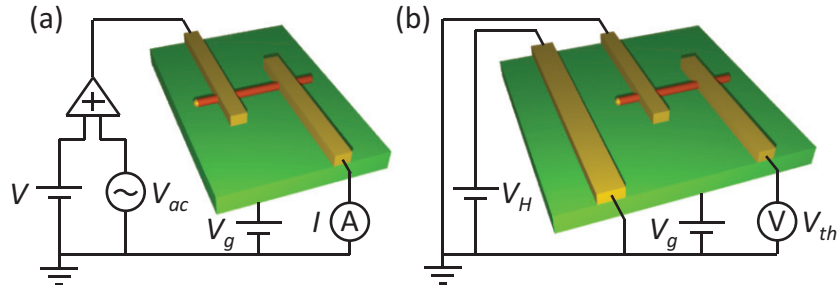
Figure 5.4. (a) Circuitry used for conductance measurements. The setup shown here is that usually used for measuring Coulomb blockade diamonds (see Chapter 6). A voltage, V, is applied to bias the nanowire. A small AC voltage (V_{ac}) is added to this so that the current, I, that is measured is directly related to dI/dV. A voltage is also applied to the back of the chip, V_g, to gate the device. (b) Circuitry used for thermovoltage measurements. A heating voltage, V_H, is applied to the heater so that a temperature gradient is created along the length of the nanowire. The resulting thermovoltage, V_{th}, is measured between the two contacts to the nanowire.

temperature in the heated contact (ΔT_H) is assumed to be proportional to the heating power, $P_H = I_H V = I_H{}^2 R$, caused by the heating current (I_H) flowing through the contact. If the heating current is an AC signal it can be written as $I_H = I_0 \cos(\omega t)$, leading to the following expression:

$$\Delta T_H \propto P_H \propto I_H{}^2 \propto \cos^2(\omega t) \propto \cos(2\omega t). \tag{3}$$

It can thus be seen that the thermal response will have twice the frequency of the heating current, resulting in the necessity of 2nd harmonic measurements. The thermoelectric response can be measured either as a thermocurrent (I_{th}), or as a thermovoltage (V_{th}). It is simpler to measure I_{th} since V_{th} must be measured under open-circuit conditions, which can be rather difficult to accomplish due to the large

impedance of the nanowire devices. The impedance of the measurement equipment must be larger than that of the nanowire for the open-circuit measurement to be valid. Quantum dot devices are especially challenging since the resistance varies considerably ($M\Omega \rightarrow G\Omega$) depending on whether the quantum dot is in Coulomb blockade or not (see Section 6.1 for an introduction to Coulomb blockade). One option when measuring V_{th} is to actually close the circuit by placing a load resistance between one end of the nanowire and ground. The measured voltage will then not be the full signal that the device produces, but this signal can be obtained if the load resistance is taken into account, as was done in Paper III (for more details see Ref. [50]). Regardless of the measurement technique, it is good practice to measure the thermoelectric response without a temperature gradient to determine whether there are any thermoelectric responses not induced by the device itself. An example of another contributor in this situation are the cables, the temperature of which varies from room temperature to the temperature of the sample space in the refrigerator. An advantage of AC thermoelectric measurements is that such unintentional DC thermovoltage in the measurement setup can be disregarded.

5.3   Thermometry

Thermoelectric measurements are closely connected to the art of thermometry. Measuring a temperature at room temperature is not considered particularly difficult. However, at the very low temperatures required in this work, it can be very challenging, especially when the distance between the two measuring points is only about a micrometer. The two methods employed during this work are presented briefly below.

5.3.1 Resistance thermometry

One method that can be used in thermometry is to simply measure the resistance of a piece of material as a function of temperature. To measure the temperature gradient along the length of a nanowire two strips of metal are required, one at each end of the nanowire. These will function as two separate thermometers and can also serve as contacts to the nanowire. Each strip has four leads, A – D as shown in Figure 5.5 (a). The thermometers must first be calibrated as a function of temperature (as shown in Figure 5.5 (b)), before thermometry can be performed. A constant current flows from A to B (so that the current passes by the end of the nanowire), and the voltage drop is measured between C and D. Estimates of ΔT are obtained by applying a heating current through the heater to create a temperature gradient along the nanowire at a specific temperature. The resistance of the two thermometers at each end of the nanowire is then measured. It is possible to measure the resistance of both thermometers at the same time if AC techniques are employed at appropriate frequencies. The increase in resistance of each thermometer resulting from the applied temperature gradient can be converted into an increase in temperature using the calibration curves. These two increased temperatures can then be used to determine ΔT. Depending on the choice of heating technique, both contacts, including the one furthest away from the heater, might suffer from an increase in temperature, and it cannot be assumed that the colder contact remains at the temperature in the refrigerator. In the work presented in this thesis, gold was used for the thermometers (the same metal as used for contacting the nanowires) in order to facilitate fabrication. This works well down to approximately 15 K, since the resistance of gold decreases
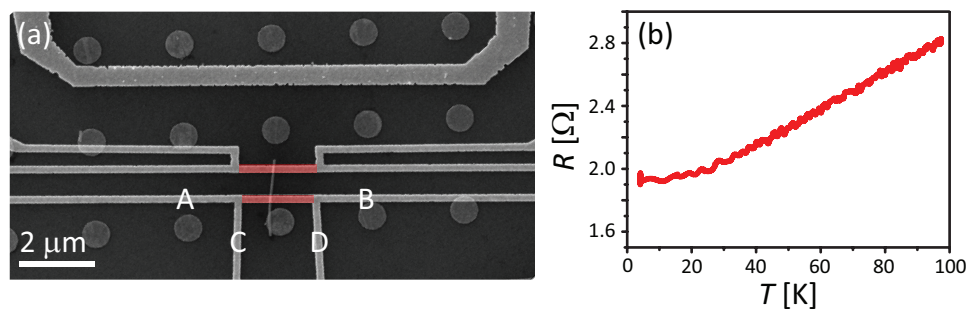
Figure 5.5. (a) A device where the contacts to the nanowire (shown in red) also function as thermometers. Each thermometer strip/contact has four leads, A-D. A constant current can be passed between A and B, and the resulting voltage drop measured between C and D. The voltage drop can then be converted into the resistance ($R = U/I$) as shown in (b), which shows the resistance of a gold strip as a function of temperature. It can be seen that at temperatures below about 15 K, the resistance is no longer a linear function of the temperature.

linearly as a function of temperature down to this value, as can be seen in Figure 5.5 (b). However, below 15 K the resistance remains more or less constant (likely due to suppressed electron-phonon interaction at lower temperatures), and this kind of resistance thermometry cannot be used below this temperature.

5.3.2 Quantum-dot thermometry

As most of the measurements presented in this thesis were performed at temperatures below 15 K, another kind of thermometry was required. The method used will be referred to as quantum-dot thermometry, and is described briefly below. For a more extensive discussion, see Refs [42, 51, 52].

Quantum-dot thermometry is based on using the quantum dot itself to measure the electron temperature on either side of the quantum dot. To do this, an energy level of the quantum dot is used to sample the Fermi-Dirac distribution of the electron gas. There are two requirements for this to be possible. The first is that the energy levels of the quantum dot must be sufficiently well separated in energy with respect to the thermal energy so that only one energy level contributes to transport through the quantum dot ($\Delta E \gg kT$). The second is that the quantum dot must be biased by a voltage, V, such that the Fermi-Dirac distribution is sampled only at the source or the drain contact. This means that the electron temperatures on the source and the drain sides of the quantum dot are measured separately, and the temperature difference between them can be calculated by subtraction. The temperatures on either side of the quantum dot are obtained by determining the ratio between the thermocurrent, I_{th}, and the second differential conductance, G_2, which is obtained by measuring the differential conductance, and then taking the numerical derivative of the measured values. The conductance measurement is needed as it provides information about the transmission function of the quantum dot. Since the energy level of the quantum dot is used as a tool in this measurement, the size of its full width at half maximum with respect to energy, Γ, is important. Different approaches are required depending on how Γ is related to kT. If $\Gamma \ll kT$, it is assumed that Γ can be approximated by a delta function, and an analytical expression for the ratio between I_{th} and G_2 can be obtained [43]:

$$\frac{I_{th}}{G_2} \approx \Delta T_{H,C} \frac{2k}{e} \left(V - V_{s,d}\right) \coth\left(\frac{e}{4k} \frac{V - V_{s,d}}{\Delta T_{H,C} + T}\right), \tag{4}$$

where $\Delta T_{H,C}$ is the difference in temperature on either the hot or the cold side of the quantum dot with respect to the background temperature T, and $V_{s,d}$ is the voltage that places the electrochemical potential of either the source or the drain contact at

45

the energy level of the quantum dot [43]. This approximate analytical expression can be compared with the measured data to extract the electron temperature.

If instead $\Gamma \gg kT$, the ratio between I_{th} and G_2 can be approximated as [51]:

$$\frac{I_{th}}{G_2} \approx \Delta T_{H,C} \frac{\left(\Delta T_{H,C} + T\right)}{\Lambda_{s,d}} \frac{4k^2}{e^2}, \tag{5}$$

and the temperature can be obtained by inserting values of this ratio into Eq. (5) above. This approach requires that the background temperature, T, during the measurement is known, and that the dimensionless scaling factor, $\Lambda_{s,d}$, has been numerically calculated. The scaling factor corrects for the approximations made to obtain Eq. (5) [53, 54]. If $\Gamma \approx kT$ it is not possible to obtain an analytical expression for the ratio between I_{th} and G_2, but the temperature on either side of the quantum dot can be predicted within an order of magnitude by combining these two approaches [51].

The attraction of quantum-dot thermometry is mainly the simplicity of using the device under investigation as the thermometer. Unfortunately, the greatest challenge in this method is the requirements on the quantum dot itself, as quantum dot devices become more complicated their functionality as a thermometer is reduced. For the method to work well, a region with ideal single-electron behavior should be used. More complicated behavior due, for example, to excited states or co-tunneling complicates the data and makes this method of thermometry difficult.

6. Electron transport through quantum dots

As a quantum dot is a 0D structure, the electrons are confined in all three spatial dimensions, and the transport of electrons to and from such a structure relies on tunneling through the potential barriers defining it. Such tunneling events will be quantized with respect to the electron charge. When studying electron transport through a quantum dot, the electrical charge of the electrons will give rise to electrostatic effects, seen as conductance peaks separated by regions of suppressed conductance. In addition, if the quantum dot is sufficiently small, the kinetic energy of the electrons will be quantized. This size quantization causes irregularities in the conductance of the quantum dot.

The concept of single-electron transport is explained briefly below, followed by a short description of the effect of size quantization on electron transport. The concept of co-tunneling will thereafter be introduced. Finally, the basics of the theoretical Landauer approach are presented in the case of defining a current through a small system, such as a quantum dot. Appropriate adjustments will also be made to the approach so that thermovoltage, thermopower and thermocurrent can be defined. Sections 6.1 and 6.2 are based on the lecture notes written by Weis [55].

6.1   Single-electron transport

The basic setup for transport measurements in a quantum dot is illustrated in Figure 6.1 (a). The quantum dot is electrically connected to two contacts: the source and the drain. It is also capacitively coupled to another electrode: the gate. The total capacitance of the quantum dot can be written as the sum of the capacitances for these contacts: $C_\Sigma = C_s + C_d + C_g$. Due to the electric charge, e, of an electron, a charging energy, $E_C = e^2/2C_\Sigma$, is required to add an electron to this quantum dot from one of the contacts. The same energy will also be required to remove an electron. The distance between the energy levels of the quantum dot, also referred to
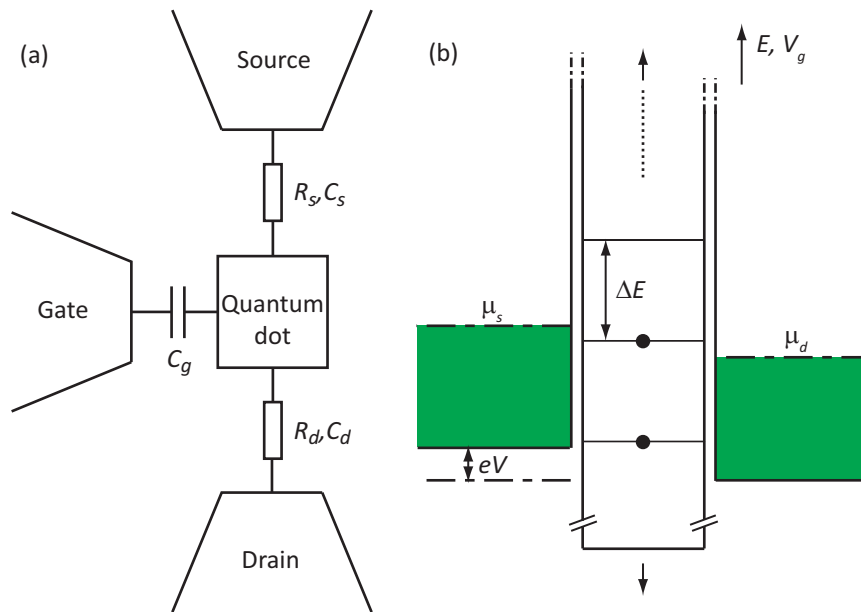
Figure 6.1. (a) A quantum dot electrically connected to a source and a drain contact, and capacitively coupled to a gate contact. (b) A voltage, V, can be applied to the source contact to open a window for transport through the quantum dot, which is the difference between the electrochemical potential of the source, μ_s, and the drain, μ_d. The energy levels of the quantum dot can be shifted up and down, as indicated by the arrows, by applying a voltage to the gate, V_g. When an energy level is situated in the energy range between μ_s and μ_d electrons can tunnel through the quantum dot from the source to the drain contact.

as the addition energy, ΔE, will therefore be $\Delta E = 2E_C = e^2/C_\Sigma$, as illustrated in Figure 6.1 (b).

If the thermal energy, kT, is smaller than ΔE, a voltage must be applied to the system for electron transport through the quantum dot to occur. The voltage, here referred to as the voltage $V = (\mu_s - \mu_d)/e$, can be applied to either the source or the drain contact. The voltage adjusts the difference between the electrochemical potential of the source (μ_s) and the drain (μ_d) contact. A voltage can also be applied to the capacitively coupled gate electrode, thereby adjusting the positions of the energy levels of the quantum dot with respect to μ_s and μ_d. This voltage will be referred to as the gate voltage, V_g. Electrons can only tunnel through the quantum dot when one of the dot's energy levels is situated between the electrochemical potential of the source and the drain as in Figure 6.1 (b). When the electrons are not allowed to tunnel through the quantum dot, they are said to be Coulomb blockaded, whereas single-electron tunneling occurs when the electrons can pass through the quantum dot one-by-one.
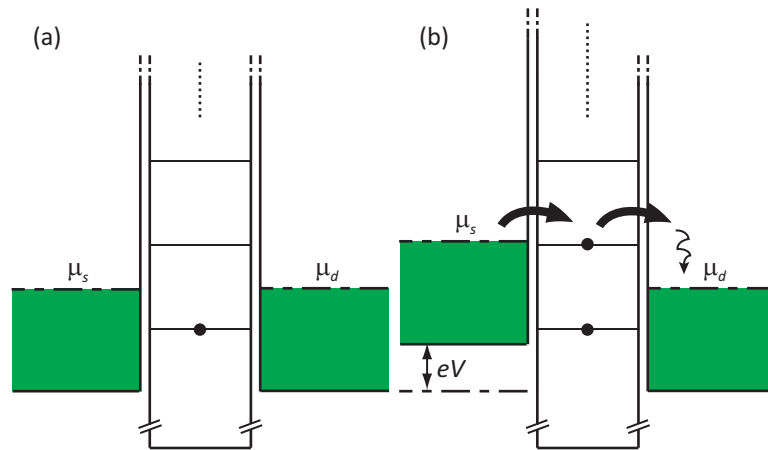
Figure 6.2. (a) This quantum dot has no energy levels between the electrochemical potential of the source (μ_s) and the drain (μ_d) contact, and electron transport is therefore blocked. (b) A large voltage, V, is applied, changing μ_s, allowing electrons to tunnel through the quantum dot.

If V_g is kept constant and a small voltage V is applied between the source and drain, the resulting current, I, will depend on where the energy levels of the quantum dot are situated with respect to μ_s and μ_d. If the system is as shown in Figure 6.2 (a), quite a large voltage V has to be applied before any electrons can tunnel through the structure (Figure 6.2 (b)). The resulting current will show a behavior similar to that of the solid line in Figure 6.3 (a). If, on the other hand, there is an energy level between μ_s and μ_d already when a small V is applied (as in Figure 6.1 (b)), the current will
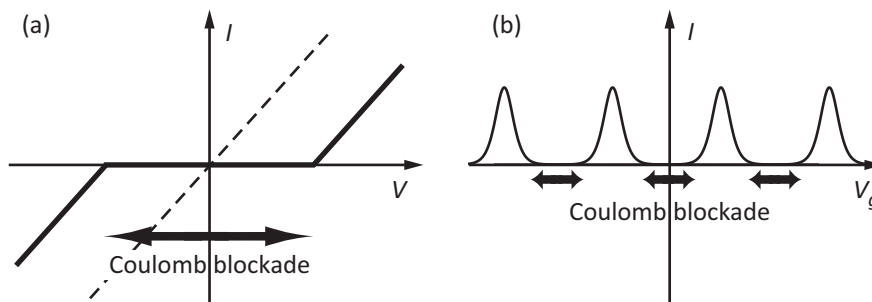
Figure 6.3. (a) Current, I, plotted as a function of voltage, V. The solid line shows the typical I-V behavior of a quantum dot which is in Coulomb blockade (indicated by the arrows). The dashed line shows the current when there is an energy level between the electrochemical potential of the source and the drain for vanishingly small applied voltages. (b) Current, I, plotted as a function of gate voltage, V_g. The graph shows the characteristic Coulomb blockade peaks for a quantum dot separated by regions of suppressed conductance (indicated by the arrows). Peaks occur as the energy levels of the quantum dot are moved through the energy window opened for electron transport by a small applied V.

49

immediately flow, as indicated by the dashed line in Figure 6.3 (a). If I is measured as a function of V_g instead, characteristic Coulomb blockade oscillations will be measured [56], as illustrated in Figure 6.3 (b). As long as an energy level is between μ_s and μ_d, current will flow through the structure, but as soon as the increase in V_g has shifted the energy level below μ_d, no current will flow until a new energy level enters the window for transport by reaching μ_s. As the plot in Figure 6.3 (b) indicates, this will result in conductance peaks separated by regions of suppressed conductance, where the peaks have the same energetic distance as that between the energy levels of the quantum dot.

Another way of characterizing the transport properties of a quantum dot is to measure the current as a function of both V_g and V. The resulting plot will show features called Coulomb blockade diamonds, as shown in Figure 6.4. The dark shaded areas represent Coulomb blockaded regions where current is suppressed. In the lighter shaded areas around these diamonds it is possible for electrons to tunnel through the quantum dot one-by-one.

Figure 6.4. Coulomb blockade diamonds seen when plotting the current, I, as a function of the voltage, V, and gate voltage, V_g. Dark shaded areas show Coulomb blockaded regions where current is suppressed. In the lighter shaded areas electrons tunnel through the quantum dot one-by-one. In the white areas V is large enough for the charge on the quantum dot to fluctuate by $\pm 2e$.
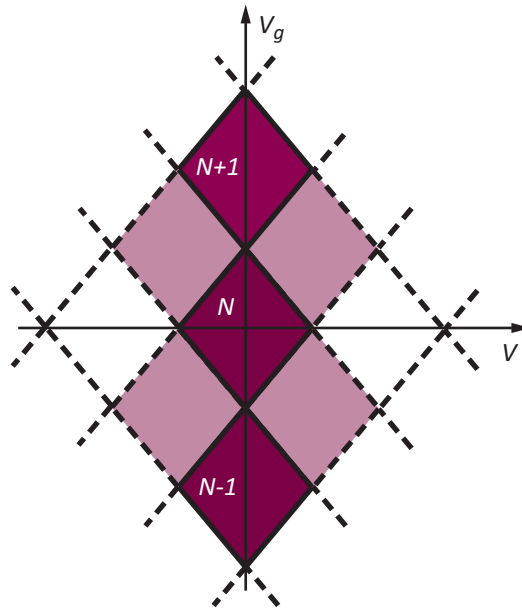
6.2 Size quantization

If the quantum dot is made so small that its size becomes comparable to the Fermi wavelength of the electrons [57], size quantization will start to influence the measurements. The kinetic energy of the electrons in the quantum dot will be quantized due to quantum mechanical effects, and this will be reflected in the Coulomb blockade diamonds when the quantization energy, $\Delta\varepsilon$, is comparable to the charging energy, E_C. The smaller the quantum dot, the larger $\Delta\varepsilon$ becomes. Signs of size quantization are variations in the size of the Coulomb blockade diamonds depending on the number of electrons on the quantum dot, as well as contributions to electron transport due to excited states. The excited states are visible as lines running parallel to, and outside the borders of, the Coulomb blockade diamonds, as can be seen in Figure 6.5 (a). The addition energy, ΔE, required to add another electron to the quantum dot will consist of both E_C and $\Delta\varepsilon$ when size quantization
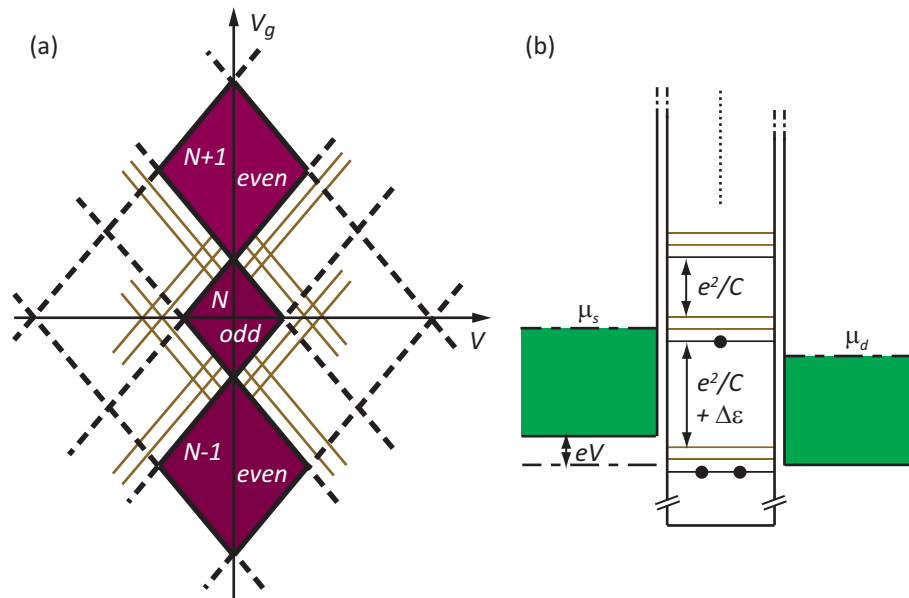
Figure 6.5. (a) Expected Coulomb blockade diamond pattern for a quantum dot when both electrostatic effects and size quantization influence electron transport. The size of the diamonds now depends on whether the number of electrons on the quantum dot, N, is even or odd. In this particular case, N is odd. The brown lines along the borders of the diamonds represent tunneling of electrons through the quantum dot via excited states. (b) The magnitude of the addition energy, ΔE, depends on whether there is an even or an odd number of electrons residing on the quantum dot when size quantization must be taken into account. The brown energy levels situated above the black ground state energy levels represent excited states.

must be taken into account. Figure 6.5 (b) indicates that a larger addition energy is needed to add another electron to the quantum dot when there is an even number of electrons residing there. This is a result of spin degeneracy; each level can be occupied by a spin-up as well as a spin-down electron. For example, adding the third electron to the quantum dot requires the addition energy $\Delta E = e^2/C_\Sigma + \Delta\varepsilon$, whereas the fourth electron only requires $\Delta E = e^2/C_\Sigma$ to be added [58].

6.3   Co-tunneling

Sequential tunneling takes place when one electron at a time tunnels to or from the quantum dot, as described above. At low temperatures, higher-order tunneling processes, known as co-tunneling processes (sometimes also referred to as virtual tunneling processes) can become important. Co-tunneling is the case when tunneling of two or more electrons occurs coherently. These processes are normally divided into one of two categories, elastic or inelastic; the difference being that inelastic processes leave the quantum dot in an excited state. Elastic co-tunneling is the dominant transport mechanism for small V, within the Coulomb blockade diamonds, as illustrated in Figure 6.6. Inelastic processes start contributing to electron transport when V is larger than the difference in energy between the ground state and the first excited state for a constant number of electrons on the quantum dot [59].

Co-tunneling dominates electron transport when first-order, single-electron transport processes are prohibited within the Coulomb blockade diamonds. It is seen as
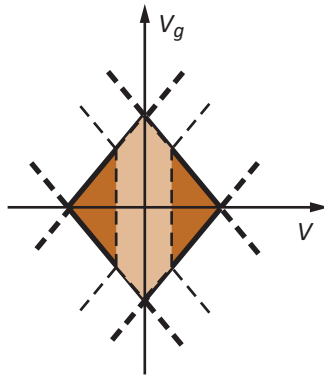

Figure 6.6. A Coulomb blockade diamond showing the contributions of elastic co-tunneling in lighter shading and inelastic co-tunneling in darker shading. Note that the onset of the contribution from the inelastic processes coincides with the signature of transport through the first excited state outside the Coulomb blockade diamond.

electrons tunneling through the quantum dot via a virtual state, hence the name virtual tunneling [60]. The full tunneling event does not change the number of charges on the quantum dot. For this to be possible, the time taken for a tunneling event must be short enough not to violate the energy–time uncertainty relation [61]. Short tunneling times can be achieved by a strong coupling between the quantum dot and the contacts, which also results in a broadening of the quantum dot energy levels [62, 63]. The amount of co-tunneling present in transport through a quantum dot therefore depends on the strength of this coupling, and increases as the coupling strength increases.

6.4 The Landauer approach

In a macroscopic system the conductance is defined as $G = I/V = \sigma(W/L)$, where I is the current through the conductor, V is the voltage drop across the conductor, σ is the material-specific conductivity, and W and L are the width and length of the conductor. This equation does not make sense for a small system, as the conductance would become infinitely large as the length of the conductor is decreased. Instead, as the length of the conductor grows shorter than the mean free path of the electrons, transport through the conductor is limited by boundary scattering. Another approach to describe transport is therefore needed, and one way to describe electron transport in small systems such as quantum dots is to use the Landauer approach. The conductance is then described by the probability of an electron being transmitted through the system [64].

Within the Landauer formalism the conductance in a small system, such as the one illustrated in Figure 6.7, at temperature $T = 0$ K, is defined as:
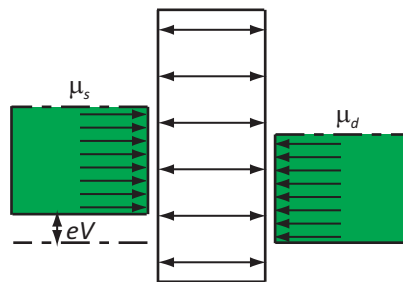

Figure 6.7. A conductor between a source and a drain contact. The arrows indicate the number of modes, M, available for transport. Note that the contacts have many more modes than the conductor.

$$G = \frac{2e^2}{h} Mt, \tag{6}$$

where e is the electric charge of an electron, h is Planck's constant, M the number of modes available for transport in the conductor, and t the average probability of an electron being transmitted through the conductor. The current through the conductor can be written as:

$$I = \frac{2e}{h} Mt(\mu_s - \mu_d), \tag{7}$$

if V is defined as $V = (\mu_s - \mu_d)/e$, where μ_s and μ_d are the electrochemical potential of the source and drain contacts. If the temperature is raised above 0 K the current is instead defined as:

$$I = \frac{2e}{h} \int \tau(E, V, T)[f_s(E, \mu_s, T_s) - f_d(E, \mu_d, T_d)] \, dE, \tag{8}$$

where $\tau(E, V, T)$ is the energy-, voltage-, and temperature-dependent transmission function (the product between the number of available modes, M, and the transmission probability per mode, t), and f_s and f_d are the Fermi-Dirac distribution in the source and drain contacts. This last equation is only strictly valid if the transmission function is independent of the direction of electron transport, i.e. $\tau(E)$ must be the same regardless of whether electrons travel from left to right or right to left.

For Eq. (8) to be used for calculations of the current through quantum dots an appropriate transmission function, $\tau(E, V, T)$, is needed. It is common to assume that $\tau(E, V, T)$ is independent of V and T, and that it can therefore be written as $\tau(E)$. A possible approximation of this function for a quantum dot is the Lorentzian approximation [64]. To account for several resonance levels, $\tau(E)$ would take the form:

$$\tau(E) = \sum_n A_n \frac{(\Gamma_n/2)^2}{(E - E_n)^2 + (\Gamma_n/2)^2}, \tag{9}$$

where A_n is the amplitude of the nth resonance of the quantum dot centered at energy E_n and with a full width at half maximum of Γ_n. Γ_n is related to the coupling strength between the quantum dot and the contacts, and therefore also to the tunneling probability.

To measure the thermoelectric response of a quantum dot, a temperature difference, ΔT, must be applied across it. Within this theoretical approach ΔT will be applied by considering the source contact to have a temperature $T + \Delta T$, whereas the drain contact remains at temperature T, as illustrated in Figure 6.8. For computational reasons, the average temperature will also be defined as: $\bar{T} = T + \Delta T/2$. In linear response, where $eV \ll k\bar{T}$ and $\Delta T \ll \bar{T}$, $f_{s/d}$ can be expanded around $\bar{T}$ and

54
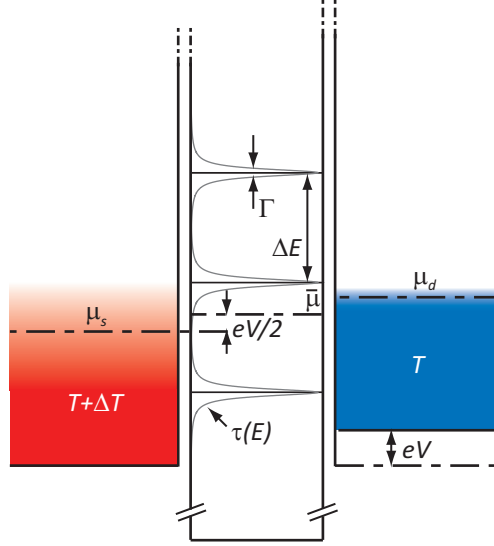
Figure 6.8. Schematic illustration of important aspects when considering thermoelectric effects in a quantum dot. The temperature on the left side of the quantum dot is raised by ΔT to $T + \Delta T$. This results in a smearing of the Fermi-Dirac distribution on the left/hot side of the quantum dot compared to the right/cold side, which remains at temperature T.

$\bar{\mu} = \mu_{s/d} \pm eV/2$, the average electrochemical potential (Figure 6.8), assuming that V is applied symmetrically across the quantum dot:

$$f_{s/d} \approx f_0 + \frac{\partial f_0}{\partial E}\left[\mp\frac{eV}{2}\pm\frac{\Delta T}{2}\frac{(E-\bar{\mu})}{\bar{T}}\right], \tag{10}$$

where $f_0 = [1 + exp(\beta)]^{-1}$ and $\beta = (E - \mu)/k\bar{T}$. The thermovoltage, V_{th}, is defined as the open-circuit voltage measured in response to the applied ΔT. V_{th} can therefore be derived from Eq. (8) under the condition that no net current is allowed to flow through the quantum dot, i.e., $I = 0$, when $\Delta T \neq 0$. If the expansion of $f_{s/d}$ in Eq. (10) is used, V_{th} takes the following form [65, 66]:

$$V_{th} = \frac{\Delta T}{e\bar{T}}\frac{\int \tau(E,V,T)\frac{\partial f_0}{\partial E}(E-\bar{\mu})\,dE}{\int \tau(E,V,T)\frac{\partial f_0}{\partial E}\,dE}. \tag{11}$$

The thermopower, $S = V_{th}/\Delta T$, is a commonly used quantity within the field of thermoelectrics, and it can easily be calculated from Eq. (11). Another measurable quantity is the thermocurrent, I_{th}, i.e., the net current flowing through the quantum dot due to an applied ΔT if the circuit is closed. Within the Landauer approach I_{th} can be defined as:

$$I_{th} = \Delta T \frac{\partial I}{\partial \bar{T}} = \Delta T \frac{2e}{h}\int \frac{\partial(f_s - f_d)}{\partial \bar{T}}\tau(E,V)\,dE, \tag{12}$$

55

if the transmission function does not depend on temperature [52]. The advantage of using thermocurrent is mainly that the voltage is constant, which simplifies the modeling.

7. Thermoelectric measurements on quantum dots

According to the Landauer picture used to derive Eq. (11) in Section 6.4, the thermopower is highly dependent on the transmission function of a quantum dot. The transmission function, in turn, depends on the distance between the energy levels of the quantum dot (ΔE) and the width of these resonances, Γ, with respect to energy (Eq. (9)). The width, Γ, is a measure of the coupling strength between the quantum dot and the contacts. It will therefore affect whether the electron transport is dominated by sequential tunneling or co-tunneling. As was shown in Chapter 6, the distance between the energy levels will depend on the relative sizes of kT, e^2/C_Σ and $\Delta\varepsilon$, and the resulting lineshape of the thermopower will therefore be affected by the size of the quantum dot and the temperature at which the measurements are performed. The lineshape of the thermopower has been studied several times over the past twenty years for differently sized quantum dots, and the first half of this chapter gives a brief review of those studies.

According to the Landauer formalism the applied source-drain bias voltage, V, must be smaller than the thermal energy kT for the current, I, to remain within linear response. This is a result of the rapidly varying transmission function of a low-dimensional system with respect to energy [64]. It should therefore be fairly easy to push transport measurements of a quantum dot out of the linear response regime by applying larger values of V, especially at low temperatures, because of the oscillating transmission function of quantum dots, see Eq. (9). The same argument can be used for thermoelectric measurements. The thermovoltage, V_{th}, is proportional to the applied temperature difference, ΔT, within linear response, but this is only strictly valid in the limit as $\Delta T \to 0$. When the applied ΔT is on the order of T it would not be surprising if deviations from linear behavior were seen, as is indeed the case, as discussed in the second half of this chapter.

7.1 Thermopower lineshapes

7.1.1 Literature review

The lineshape of the thermopower of a quantum dot was theoretically calculated for the first time in 1992 [67]. The thermopower was predicted to oscillate around zero with the same period as that of the Coulomb-blockade oscillations seen when measuring conductance (as shown in Figure 7.1). The calculations also predicted that the thermopower would oscillate around zero in a sawtooth-like manner (Figure 7.1 (a)), with a maximum thermopower, $S^{max} = \Delta E/4eT$. Two major assumptions were made during the calculations. The first was that all virtual tunneling processes, and thus the resulting widths of the transmission resonances of the quantum dot, could be neglected; and the second was that the electrostatic energy could be described by the classical charging energy, $E_C = e^2/2C_\Sigma$.

This theoretical model was soon thereafter compared with experimental results obtained by measuring the thermoelectric properties of quantum dots defined in 2DEGs by Staring et al. [14] and Dzurak et al. [68]. Both groups confirmed that the thermovoltage indeed oscillates with the same period as that of the Coulomb blockade peaks found in conductance, and that the thermovoltage exhibits a sawtooth-like lineshape, similar to that shown in Figure 7.1 (a). The measurements by Staring et al. were performed at low temperatures ($T = 300$ mK and lower), $kT \ll e^2/C$, and with small heating currents, resulting in ΔTs estimated to be about 1 mK. Reasonable qualitative agreement was obtained with the theory, but the amplitude of the measured thermovoltage was smaller than that predicted. To obtain quantitative agreement it was necessary to overestimate the temperature by a factor of five compared to the actual temperature of the measurement. This discrepancy was suggested to be the result of the finite width of the resonance levels in the quantum dot.

Dzurak et al., on the other hand, estimated their heating currents to result in ΔTs of about 1-2 K compared to the measurement temperature of 550 mK; well within the nonlinear heating regime ($\Delta T > T$). Despite this, they found reasonable agreement with a linear response model based on the Mott relation [69] when using the average temperature, $\bar{T}$. When comparing their results to the theoretical model by Beenakker and Staring they found their thermovoltage amplitudes to be one order of magnitude smaller than those predicted, which they also considered to be the result of broadening of the resonance levels of the quantum dot. Dzurak et al. [70] published another set of thermovoltage measurements in 1997, still in the nonlinear regime, but at a lower background temperature of 50 mK. Again, they found much smaller
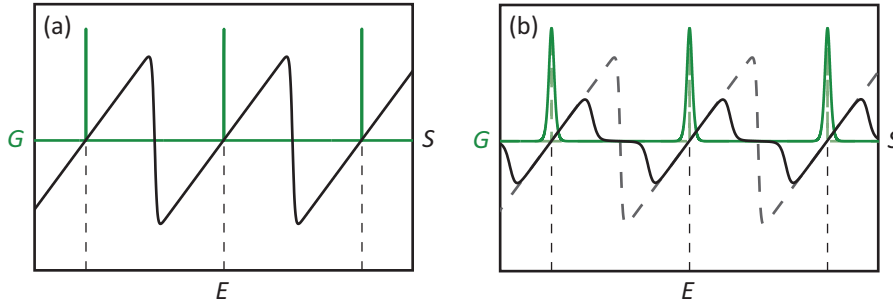
Figure 7.1. Conductance, G, and thermopower, S, as a function of energy, E. (a) For conductance peaks that have no width (delta functions) S assumes the sawtooth-like shape predicted by Beenakker [67]. (b) If the conductance peaks have a certain full width at half maximum, Γ, S assumes a more derivative-like shape, with regions of zero S between the conductance peaks due to co-tunneling [71].

amplitudes of the thermovoltage, by two orders of magnitude, than predicted by the theory presented by Beenakker and Staring, whereas reasonable agreement was found with a single-particle Landauer formulation. Their interpretation was that the lineshape of the thermovoltage must be seriously affected even by small amounts of co-tunneling.

In an effort to create a model that fitted the experimental results more accurately, a theory including co-tunneling was developed by Turek and Matveev [71]. The system modeled was a single-electron transistor based on a quantum dot, weakly coupled to its two leads. Turek and Matveev took into consideration that co-tunneling processes would dominate conductance in the valleys between the Coulomb blockade peaks below a certain critical temperature. This would strongly affect the thermopower, which reaches its maximum values near the centers of these valleys. As the temperature is lowered, the model indeed predicted a transition from a sawtooth-like lineshape to a lineshape more similar to the derivative of the conductance, with regions of completely suppressed thermopower between the conductance peaks, as shown in Figure 7.1 (b).

In measurements on a quantum dot defined in a 2DEG performed by Scheibner et al. [72] the transition from the sawtooth-like lineshape to a derivative-like one was indeed seen when lowering the temperature, in agreement with the theory of Turek and Matveev. There were, however, some deviations between the measurements and theory; the peak positions and amplitudes of the thermovoltage did not agree well with those predicted by the theory. This was considered to be the result of the sequential tunneling regime extending further into the valleys between the conductance peaks of the few-electron quantum dot used in the measurements, compared to the many-electron quantum dot considered in the theory.

The effect of Γ on the lineshape of the thermopower has been thoroughly discussed in the literature, but complete agreement between theory and experimental results has proven elusive. A change in T has been used to change the amount of co-tunneling expected to contribute to transport through the quantum dot, but the effects of a change in T on ΔE have not been considered. In an attempt to solve these problems and other unanswered questions, a study was carried out on the lineshape of the thermopower of quantum dots, which is described in Paper III.

7.1.2 The present work
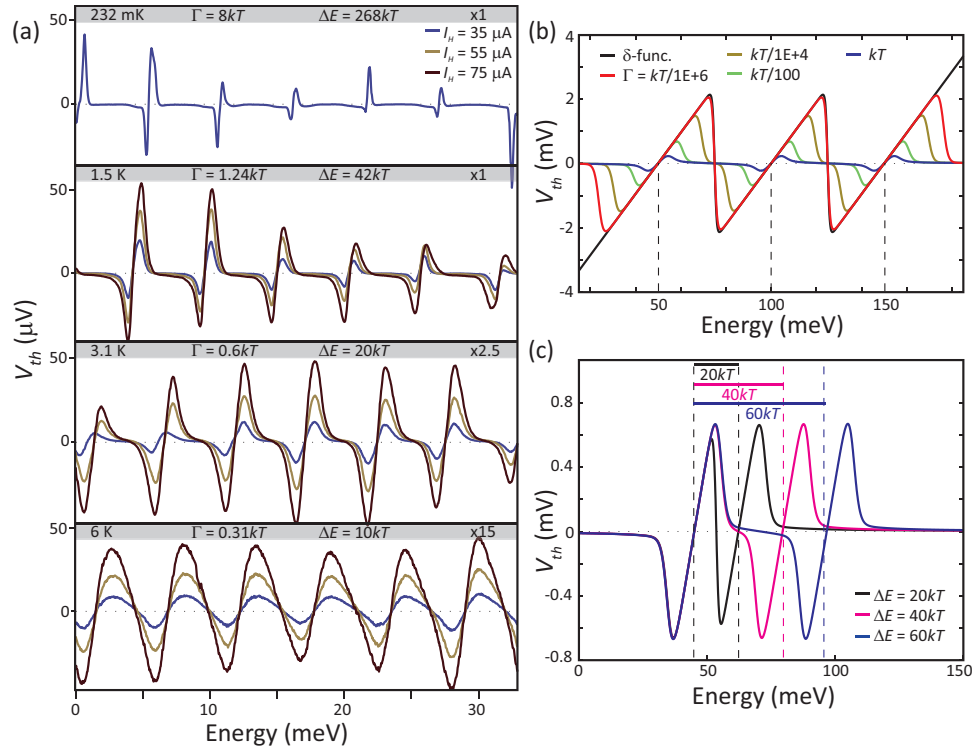
Figure 7.2. (a) Measurements showing how the lineshape of the thermovoltage, V_{th}, changes as the temperature T is increased. Data are shown for different heating currents, I_H, for each temperature. As T is changed the relationship between the broadening of the energy levels, Γ, and the thermal energy kT, as well as the distance between the energy levels, ΔE, and kT change. (b) Modeling based on the Landauer approach shows how the lineshape of V_{th} changes as Γ is increased for a fixed value of $\Delta E = 50$ meV $\approx 58kT$ ($T = 10$ K and $\Delta T = 1$ K). (c) The change in lineshape of V_{th} as ΔE is increased for a fixed value of $\Gamma = kT/100$ ($T = 10$ K and $\Delta T = 1$ K) based on the Landauer approach. (The figure has been adapted from Paper III.)

The thermopower lineshape of quantum dots defined in heterostructure nanowires was systematically investigated with respect to $\Delta E/kT$ and Γ/kT as a function of temperature (Paper III). The aim of the investigation was to gain an understanding for how the lineshape relates to the transmission function of a quantum dot, and to examine if it was possible to predict the lineshape using a transmission function extracted from standard conductance measurements. When changing the two energy scales $\Delta E/kT$ and Γ/kT, by increasing the temperature in the measurements, a transition from a derivative-like lineshape to a more triangular-looking lineshape was oberved (as shown in Figure 7.2 (a)). Comparison with a simple Landauer-type model, using a transmission function based on experimental measurements, indicated that the main cause of the change in lineshape was the decrease in $\Delta E/kT$ when increasing the temperature (see Figure 7.2 (b) and (c)). When including the effects of the measurement setup in the modeled data, excellent qualitative and reasonable quantitative agreement were found between measurements and calculations. The different parameters that influence the transmission function of a quantum dot (kT, ΔE, Γ) do indeed have a considerable effect on the resulting lineshape of the thermopower. It is, however, possible to predict the thermopower lineshape from the simple Landauer-type model used in Paper III, if these parameters are extracted from standard conductance measurements.

7.2 Nonlinear effects

7.2.1 Literature review

Deviations from the expected linear behavior of the thermopower as a function of applied thermal gradient were reported already in the first publication on thermopower measurements on a quantum dot defined in a 2DEG by Staring et al. in 1993 [14]. Most remarkable was the observation of a sign change of the amplitude of V_{th} as the heating current was increased. Figure 7.3 shows examples of such nonlinear behavior from our own measurements, using a nanowire-based quantum dot device. The authors of Ref. [14] estimated that the values of ΔT were much larger than both T and $\Delta E/k$ at the heating current for which the sign change occurred, and therefore considered that the measurements were beyond the regime of linear response. Measurements of the thermovoltage in the nonlinear regime were published in the same year by Dzurak et al. [68], who also reported a sign change of V_{th} with increased heating current. They explained this as being the result of the electrons having such large temperatures that they could be thermally excited over the electrostatic barriers defining the quantum dot in the 2DEG.
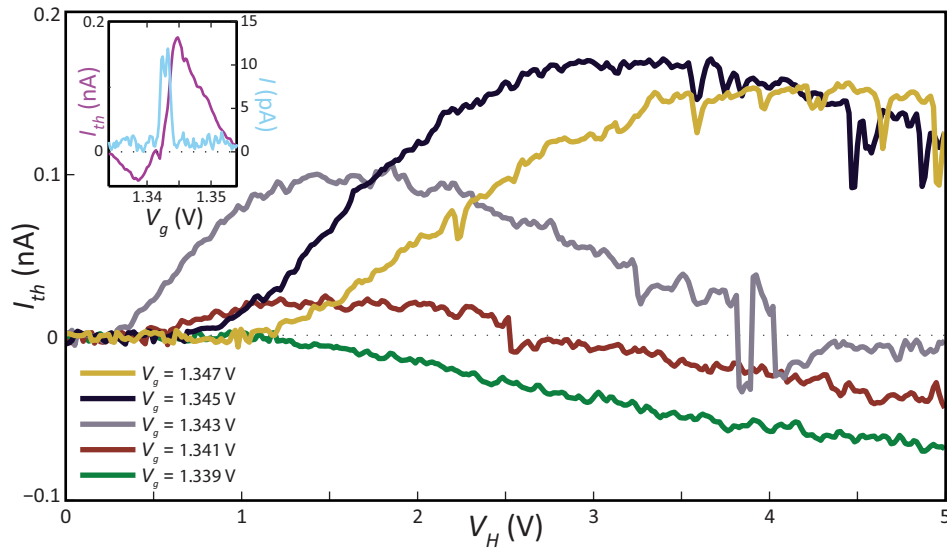
Figure 7.3. The thermocurrent, I_{th}, measured as a function of heating voltage, V_H, for five different gate voltages, V_g, at a background temperature of 13 mK. The inset shows I_{th} as a function of V_g for $V_H = 2.884$ V together with the current, I, in the same V_g region without any heating applied. The data were obtained from an InAsP quantum dot defined in an InAs nanowire by InP barriers.

Sign changes were also observed with increasing heating voltage by Pogosov et al. for a quantum dot defined in a suspended semiconducting membrane [73]. Two possible explanations were proposed. The first was that tunneling due to the absorption of phonons may still possible, even if a quantum dot is in Coulomb blockade. If the tunneling barriers are asymmetric the sign of the resulting current will be decided by this asymmetry rather than the sign of the temperature gradient. The second was that ballistic re-reflection of the electrons from the "walls" of the quantum dot could generate a current in the opposite direction to that caused by the temperature gradient. Transport through the quantum dot would then be highly dependent on the geometry of the quantum dot.

Nonlinear behavior in the thermovoltage of a quantum dot have thus been reported on several occasions in the literature in different quantum dot systems, but no physical phenomenon explaining this rather drastic behavior had been suggested, and no theoretical modeling had been performed. To address this, a thorough investigation of the nonlinear effects in quantum dots was initiated. This work is described in Paper IV.

62

7.2.2 The present work

Measurements of the thermovoltage and the thermocurrent of quantum dots defined in nanowires showed nonlinear effects, including sign changes with increased ΔT (see Figure 7.3 and Paper IV). In an attempt to find the cause of this nonlinear behavior, the data were compared with a model based on the Landauer approach. The model considers the effect of an energy-dependent transmission function, and does indeed predict nonlinear behavior of the thermocurrent with increasing ΔT. However, the nonlinear effects predicted by the model were not nearly as strong as those seen in the experimental data, and no sign changes were predicted with realistic transmission functions.

After studying the measurements in more detail, there was reason to believe that including a temperature dependence in the transmission function could explain the nonlinear behavior. In fact, a shift of the energy level of the quantum dot with respect to the gate voltage explains the nonlinearities seen in the measurements. This shift occurs as a function of ΔT, or possibly T, which also increases with increasing ΔT. To test this hypothesis, the position of the energy level of the quantum dot was given a linear dependence on ΔT in the model. The model then predicted similar sign changes in the thermovoltage as a function of ΔT to those seen in the experiments, demonstrating that shifts of energy levels of a quantum dot with respect to gate voltage are of the utmost importance in understanding nonlinear behavior in thermoelectric measurements. Figure 7.4 illustrates why a shift of the energy level with respect to the gate voltage explains the nonlinear behavior reported in Paper IV. The figure shows a data set where the shift occurs due to an electrostatic shift of the energy level with respect to the gate voltage, and not due to an increase in ΔT or T as in Paper IV. Such a sudden shift makes it easy to see the effect on the thermocurrent.

A possible reason for a shift of an energy level, in this case the shift seen for the InSb quantum dot, was also proposed in Paper IV, based on studying how the nature of the transport excitations on the quantum dot could be altered by the thermal bias applied. More measurements are needed to confirm the interpretation, especially measurements to determine whether the renormalization occurs in response to the change in ΔT, or if it is an effect of the simultaneous change in T caused by the heating techniques used. It can be concluded, however, that the results underline the importance of including temperature dependence in the transmission function when investigating the nonlinear behavior of thermoelectric effects in quantum dots. In the measurements presented here, the temperature dependence seems to be the main cause of the observed effects.
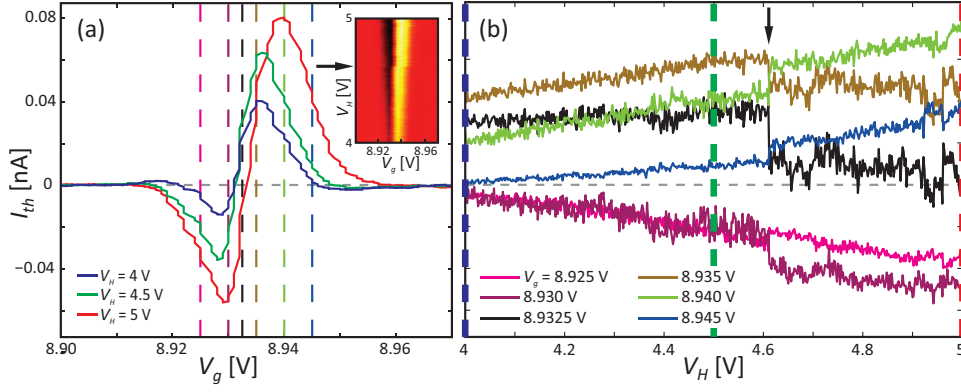
Figure 7.4. (a) Thermocurrent, I_{th}, as a function of gate voltage, V_g, for three different heating voltages, V_H. The inset shows the 2D scan with I_{th} as a function of both V_g and V_H. At $V_H \approx 4.6$ V (indicated by the arrow) a shift of the energy level with respect to the gate voltage occurs (this unfortunately happens sometimes during measurements). This is mirrored in the data shown in (a), where the two traces below $V_H \approx 4.6$ V cross zero at the same place, whereas the zero-crossing for $V_H = 5.0$ V has shifted to a higher value of V_g. (b) I_{th} as a function of V_H for different values of V_g (the positions of the different values of V_g are indicated by the dashed lines in (a)). The shift that occurs at $V_H \approx 4.6$ V (indicated by the arrow) results in a dramatic change in I_{th}, showing the important dependence of where the energy level is situated with respect to V_g in this kind of measurement. The data were obtained from an InAs quantum dot defined in an InAs nanowire at a background temperature of 300 mK.

Another explanation for nonlinear features in thermocurrent and thermovoltage as a function of thermal bias has recently been suggested by Sierra and Sánchez [74]. They considered a two-level quantum dot system and nonlinear effects were predicted as the applied thermal bias was increased. In this case, the nonlinear behavior is not the result of shifts of the energy levels, but rather the result of competing transport in different directions for the two levels of the quantum dot. The model assumed that the Fermi energy is positioned between the two energy levels, and the competing transport is thus the result of electrons travelling in one direction at the energy level above the Fermi energy, and in the other direction at the energy level below the Fermi energy. Sign changes in the thermoelectric response were also predicted in this case, and the zero-crossings were the result of equal numbers of electrons travelling in the two directions at the two energy levels. The requirement for such behavior is simply that the applied thermal bias, kT, must result in a sufficiently high thermal energy for electron transport to take place via both energy levels at the same time [74]. Performing 2D scans as a function of heating voltage and gate voltage provides a straightforward way of differentiating between the two kinds of nonlinear behavior in measurements, as shown in Figure 7.5. The shift of the zero-crossing of the thermocurrent with respect to the gate voltage can be clearly seen in Figure 7.5 (a) when heating one end of the nanowire, whereas there is no such shift if heating is

64
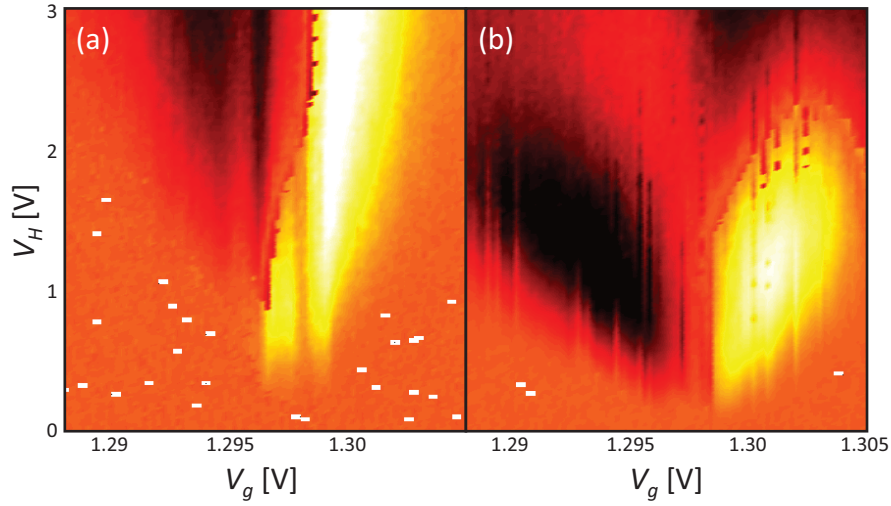
Figure 7.5. 2D scans of the thermocurrent with respect to the gate voltage, V_g, and heating voltage, V_H, for an InAsP quantum dot defined in an InAs nanowire. The measurements were performed at 13 mK. (a) The thermocurrent changes from -100 pA (black) to +100 pA (white). (b) The thermocurrent changes from -300 pA (black) to +300 pA (white).

applied at the other end (Figure 7.5 (b)). These data were obtained from a device utilizing the top-heating technique developed in the present work, see Section 4.2.3. This heating technique results in a much smaller increase of the surrounding temperature than previously used techniques, as only small heating powers are needed to obtain large temperature differences. This was probably an important reason in making it possible to observe this effect in these measurements.

8. Thermoelectric measurements as a characterization tool

The field of thermoelectrics has traditionally focused on the possibility of transforming a temperature difference into useful energy as efficiently as possible [2, 4]. Quantum dots are interesting in this context because of their energy filtering effects [10, 13, 75], which are tunable and easy to characterize, making quantum dots useful as model systems. However, in addition, thermoelectric measurements can also be considered a complementary tool to conductance measurements in characterizing a structure. The thermoelectric response may thus provide a diagnostic tool aiding the investigation of fundamental physics phenomena, and the development of the next generation of electronic and optoelectronic devices [76].

As pointed out in Section 7.2, the strongly nonlinear effects seen in thermovoltage and thermocurrent when increasing the applied thermal bias can be explained by renormalization of the energy levels of the quantum dot. Having understood this relationship between nonlinearities in the thermoelectric response and the position of the energy level, the knowledge could be used to investigate the occurrence of level shifts due to an increase in temperature or thermal bias in quantum dots. It would be impossible to explore these phenomena using only conductance measurements if the shift occurs when the applied thermal bias is changed, and would be rather cumbersome if the shift were the result of an increase in temperature, especially for a small range in temperature.

Other aspects of the thermoelectric response could also be useful; for example, the thermopower is related to the average energy of the particles contributing to transport, $S = \langle E \rangle / eT$ [77]. Another interesting aspect is that the thermopower is proportional to the energy derivative of the transmission function, in contrast to the conductance, which is proportional to the transmission function itself [69, 78]. This is only strictly true when the transmission function varies slowly as a function of energy, which is technically not the case in quantum dots. However, the relationship still implies that thermopower is a more sensitive tool when investigating transmission functions. Other examples of the usefulness of thermoelectric measurements are that it is possible to deduce the dominant charge carriers simply by determining the sign

of the thermopower [79], and that the thermoelectric signal remains non-zero in regions where conductance vanishes [72]. A short review of the use of thermoelectric measurements as a complement to conductance measurements taken from the literature is given below, followed by two examples of the application of thermoelectric measurements in the work described in this thesis.

8.1 Examples from the literature

The first theoretical publication on the thermopower of a quantum dot showed that such measurements could provide a useful complement to the more commonly used conductance measurements [67]. When modeling the thermopower in the quantum limit where $kT \ll \Delta\varepsilon$, a fine structure appears on top of the sawtooth-like lineshape described above. This fine structure has a periodicity of $\Delta\varepsilon$, the difference in energy between the ground state and the excited states for a constant number of electrons on the quantum dot, whereas the sawtooth-like lineshape has a longer periodicity of $\Delta\varepsilon + e^2/C$, i.e., the energy required to add another electron to the quantum dot. A corresponding fine structure is also present in conductance, but there it is not visible because it is so small compared to the conductance peak itself. Dzurak et al. measured a fine structure in the thermopower for their quantum dots using thermovoltage measurements, and employed Coulomb blockade spectroscopy to confirm that the fine structure in V_{th} was on the same order of magnitude in energy as that found for the excited states [70, 80]. They thereby verified that thermoelectric measurements can be a useful complement to the more frequently used conductance measurements when characterizing a new system. Kristinsdóttir et al. have in fact recently shown theoretically that the possibility to detect excited states in the thermopower can be utilized to study many-body effects. Specifically, they demonstrate that the thermopower is a tool for detection of the onset of Wigner localization of electrons in a nanowire segment [81].

Thermoelectric measurements have also been shown to be useful in various contexts. One example is in the investigation of the transport properties of quantum dots [82-84]. The dependence of the lineshape and amplitude of the thermopower on E_C/kT, originally shown by Beenakker and Staring [67], has been used by Möller et al. [82] to study how changes in the transmission probability of one of the electrostatic barriers defining a quantum dot in a 2DEG affect the charging energy of the quantum dot. By fitting thermopower data to theory [67], with E_C/kT as the only variable parameter, they were able to confirm theoretical predictions of the charging energy and its behavior with respect to transmission probability [82]. Thermopower measurements have also been shown to be useful when measuring chaos in quantum

dots. Corrections due to ohmic heating can be avoided since no current flows through the sample during a thermovoltage measurement. Corrections due to short trajectories, weak localization, and dephasing can also be ignored, as such effects were found to be absent in thermopower measurements. The theoretically predicted non-Gaussian distribution of fluctuations was therefore easily observed using thermopower measurements, while this is difficult in conductance measurements [84].

Thermopower has also been used to study the effect of Kondo correlations in a strongly coupled quantum dot [85], offering more information than can be obtained with conductance measurements. The normal sign change in the thermovoltage for each peak in conductance turns out to be absent in the strong coupling regime where Kondo correlations are present; the thermopower is only positive in these regions. If the temperature is increased, the sign change reoccurs, similarly to the disappearance of the zero bias peak with increasing temperature in conductance, a typical feature of the Kondo effect. This behavior is a strong indication that the absence of the sign change in thermovoltage is related to the Kondo correlations. The sign of the anomalous thermovoltage indicates whether the contributing transport process is electron- or hole-like, and thermovoltage measurements thus provide information that cannot be deduced from conductance measurements.

The above examples were all concerned with studies of physical phenomena in quantum dots, where thermopower measurements have been used to confirm theoretical predictions or to investigate interesting behavior in conductance in order to obtain further information. However, another interesting trend is arising, where thermoelectric measurements are being combined with conductance measurements to extract the properties of nanowires such as the Fermi level [79, 86], charge carrier mobility [79, 87], charge carrier concentration [79], and relaxation time [79]. This approach is advantageous over pure conductance approaches for various reasons. For example, there is no need to estimate the capacitance between the nanowire and the back gate, which is rather complicated [79], and it does not suffer from errors due to hysteresis effects, as do commonly used field-effect approaches [79, 87].

8.2 Characterization of quantum dot-like states in nanowires

A nanowire is considered ideally to be a 1D object. Its conductance is therefore expected to be quantized in steps of $2e^2/h$ due to its DOS [57] (Figure 8.1 (a)). This behavior has been observed for 1D constrictions defined in 2DEGs [21, 22], but it is much more difficult to see in nanowires [88]. The conductance through a nanowire
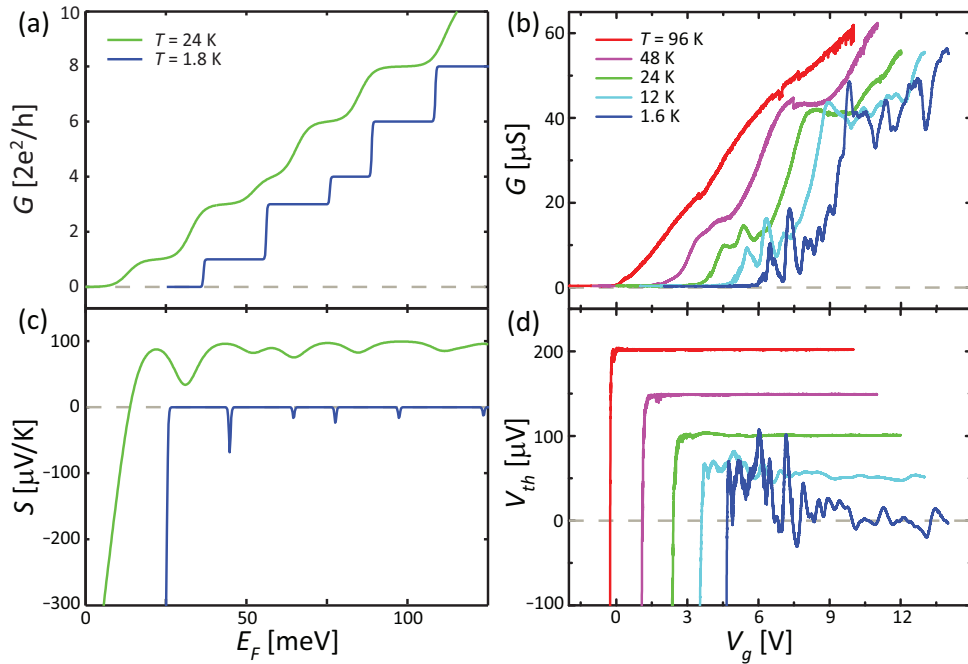
Figure 8.1. (a) Modeled conductance, G, as a function of Fermi energy, E_F, for a 50 nm diameter nanowire. Data are presented for two different temperatures, T. The trace at $T = 1.8$ K has been offset by 25 meV in E_F for clarity. (b) G, measured for a 69 nm diameter InAs nanowire as a function of gate voltage, V_g, for five different values of T. The traces have been offset by 1 V each in V_g for clarity, and only the trace at $T = 96$ K is shown with its true value. (c) Modeled thermopower, S, as a function of E_F for the same nanowire and temperatures as in (a). The results from the model have again been offset in E_F in the same way as in (a). S has also been offset, 100 μV/K has been added to the trace at $T = 24$ K for clarity. (d) Thermovoltage, V_{th}, ($V_H = 1$ V) for the same nanowire as in (b). Again the traces have been offset in V_g for clarity. They have also been offset in V_{th} with increments of 50 μV, and only the trace at $T = 1.6$ K is shown with its true value. Prof. Xanthippi Zianni is gratefully acknowledged for the modeled data.

usually has the appearance shown in Figure 8.1 (b). In fact, the observation of quantized conductance in nanowires is a somewhat debated topic, and many publications have been met with skepticism. One way to strengthen an observation of quantized conductance due to 1D confinement would be to also measure the thermoelectric response of the device. Theoretical predictions [89], later confirmed by measurements in 2DEGs [90, 91], show that the thermopower of a 1D constriction would exhibit a peak every time the conductance increases, and would be zero when the conductance is constant, as shown in Figure 8.1 (c). The observation of such peaks together with corresponding quantized conductance steps would provide strong evidence of the much sought-after 1D behavior of nanowires. However, since the conductance of a nanowire rarely exhibits clear 1D behavior, neither does the thermovoltage (Figure 8.1 (d)).

70

One way of gaining a better understanding of the measured data for a nanowire is to compare the results of thermoelectric measurements with those from conductance measurements, as was done in the present work (Paper V). The thermovoltage data for InAs nanowires, especially at low temperatures, exhibit a feature that is normally associated with thermoelectric measurements on quantum dots: i.e., the thermovoltage changes sign as a function of gate voltage, V_g, (Figure 8.2 (b)). Comparing such data with conductance measurements reveals that the sign changes occur at the same gate voltages as distinct peaks in the otherwise fluctuating conductance (Figure 8.2 (a)). This is the typical thermoelectric signature of a quantum dot, as discussed in Section 7.1. To investigate this further, Coulomb blockade diamond spectroscopy can be performed in regions around such sign changes by measuring the conductance as a function of V and V_g, as described in Section 6.1. Features similar to normal Coulomb blockade diamonds, which occur for quantum dots, are then obtained (Figure 8.2 (d)). These two features of the measurements: the alignment of sign changes in V_{th} with peaks in G; and the diamond-like features occurring in Coulomb blockade spectroscopy, strongly suggest that there is some kind of quantum dot-like states in the nanowires, although no barriers to form quantum dots were deliberately introduced during growth or fabrication. Having found these quantum dot-like states in nanowires in the present work, explaining the observed measurements, the obvious question is whether they can be utilized in any way.

It has been theoretically predicted that 1D electron confinement effects should increase the power factor $S^2\sigma$, a function of thermopower and conductivity, in nanowires [7]. This would be beneficial for thermoelectric efficiency. However, these predictions have not yet been realized experimentally due to the lack of clear 1D signatures in conductance and thermopower for nanowires. Another reason is the necessity to carefully tune of the Fermi level to just below the lowest occupied subband [92], which requires good gating capabilities in these devices. It has also been predicted that it should be possible to achieve an increase in power factor by modulating the width of the nanowire [93, 94]. These width modulations could be regarded as an attempt to introduce weakly defined quantum dots (similar to the quantum dot-like states observed in the present measurements) into the nanowires, thereby making interference possible between quasi-localized and propagating electron states. These interference effects are the reason for the expected power factor enhancement.

An increase in power factor can indeed be seen in InAs nanowires showing signatures of quantum dot-like states at low temperatures (Figure 8.2 (c)). The measurements agree qualitatively very well with the theory of power-factor enhancement due to interference between propagating and quasi-localized states (Paper V). This new

71
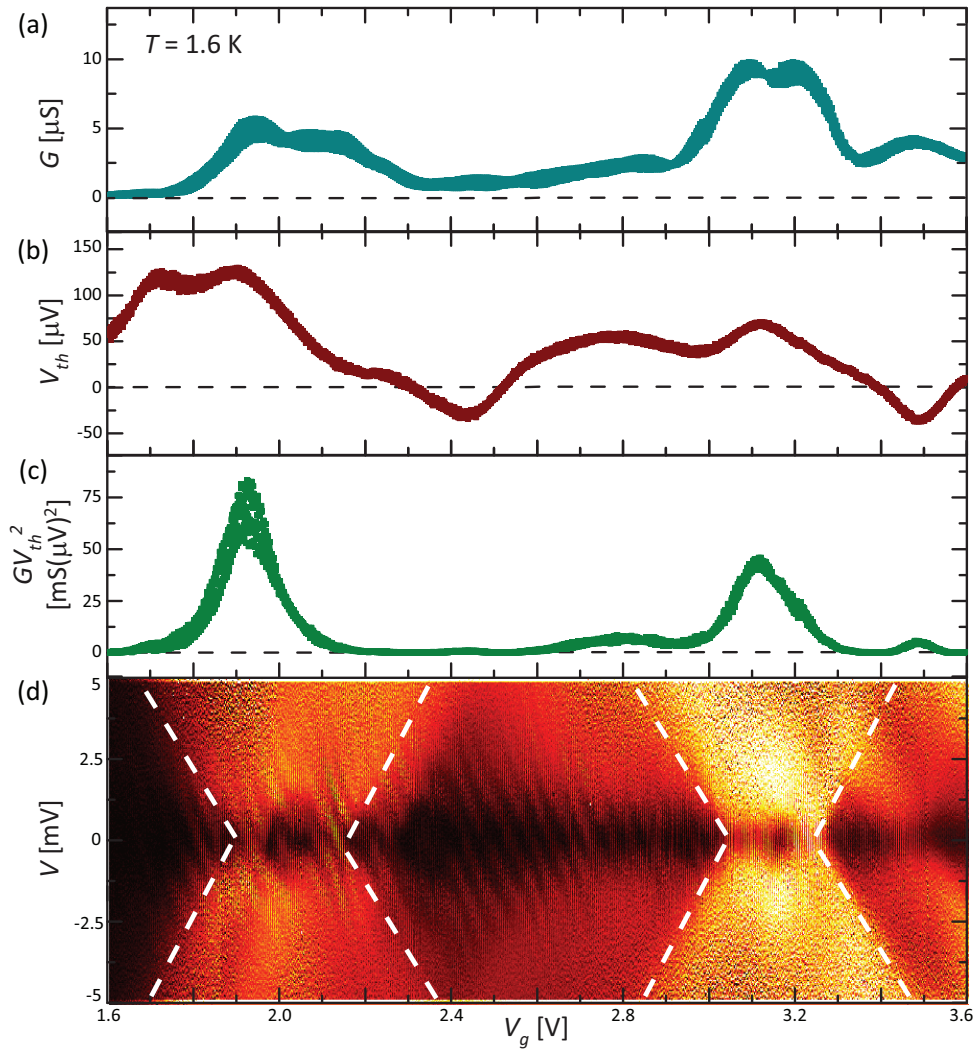
Figure 8.2. (a) Conductance, G, for the same nanowire as shown in Figure 8.1 (b) and (d), but for a smaller range in V_g, where peaks in conductance can be seen ($T = 1.6$ K). (b) Thermovoltage, V_{th}, in the same V_g region ($V_H = 1$ V). Note the sign changes at $V_g = 2.3$, 2.5, and 3.4 V. (c) GV_{th}^2 (proportional to the power factor) calculated from the data shown in (a) and (b). Peaks occur in the same regions of V_g as the quantum dot-like state features in G and V_{th}. (d) Coulomb blockade spectroscopy in the same V_g region. The dashed white lines indicate the diamond-like structure that can be seen for this InAs nanowire device.

mechanism, of utilizing quantum dot-like states in nanowires to enhance the power factor, is a promising method for industrial applications. It is promising as it allows for the use of thicker, more robust nanowires, and since fine tuning of the gate voltage (required for 1D conductance enhancement) does not seem to be as necessary

72

to obtain acceptable enhancement of the power factor. This is essential if nanowire arrays are to be used in future thermoelectric devices.

8.3 Characterization of polymer electrolyte-gated nanowires

The importance of being able to gate a nanowire for high thermoelectric efficiency was mentioned in the previous section. Gating is already a well-studied subject since it is also essential for transistors [95]. Nanowires are often gated by a back gate [96, 97], but there are other methods. Examples are nanoscale metal gates below [98], across [99], or wrapped cylindrically around, the nanowire [100-102]. It has recently been found that a polymer electrolyte gate may be the most efficient to date [103, 104]. This relies on gating via the formation of electric double layers at the interfaces between the nanowire and the polymer electrolyte, as well as between the electrolyte and the metal electrode to which the gate voltage is applied, due to ion migration [105]. The polymer electrolyte has one especially interesting feature: the ion distribution in the electrolyte 'freezes' at temperatures below 220 K since the ions can no longer move [106]. This means that the charge environment very close to the nanowire is fixed. The effect of such a fixed charge environment on a nanowire was investigated in the present work (Paper VI).

The nanowire device was cooled from room temperature to subkelvin temperatures with different settings of the polymer electrolyte gate. It was shown that the onset of conductance could be shifted by more than 5 V in the back-gate voltage V_g by changing the voltage applied to the polymer electrolyte before cooling. The amount of current flowing through the nanowire at low T also decreased by a factor of 100 as the applied voltage was changed from +500 to -1000 mV before cooling. Upon inspecting the V_g region just after the nanowire started to conduct, different behavior was seen with different polymer electrolyte settings. For positive polymer electrolyte gate voltages, the nanowire showed very stochastic Coulomb blockade peaks, which changed and shifted from one V_g sweep to V_g sweep to the next, while for negative voltages, the nanowire showed stable Coulomb blockade. This region was investigated more closely by obtaining conductance traces at different temperatures, and by performing Coulomb blockade spectroscopy and thermovoltage measurements at different temperatures (such a set of measurements is shown for another nanowire device in Figure 8.3). The measured data show a number of interesting features: 1. different T dependence for different conductance peaks, and an overall oscillation in the magnitude of the conductance peaks; 2. two interlaced patterns of diamonds in

Coulomb blockade spectroscopy; and 3. an overall oscillating thermovoltage background, resulting in an overall positive or negative thermovoltage in some regions. These features strongly resemble the behavior of a double quantum dot, where one of the dots is much more strongly coupled to its lead than the other one. Modeling was performed for such a system, and the resemblance between measured and simulated data was good.

It is not completely understood why a nanowire can behave like a double quantum dot, but these findings are interesting as they confirm the compatibility of polymer electrolytes with thermoelectric measurements. This may constitute a step towards making nanowires that can be used in cooling applications at low temperatures. As described in Paper V, an increase in power factor was seen at low temperatures in nanowires containing quantum dot-like states. Although the need for appropriate gating is not as strong as for 1D power factor enhancement-based devices, a device utilizing quantum dot-like states would still benefit from being gated into its most optimum operation region. The electrolyte gate could perhaps even be used to control the disorder found in the nanowires, which is the most likely reason for the quantum dot-like states, and to optimize it. As the polymer electrolyte gate is well-suited for thermoelectric devices due to its low thermal conductivity, it is possible to imagine an array of nanowires embedded in such a polymer. This device could then be cooled with an appropriate voltage setting so that it 'freezes' in the most beneficial way for the array of nanowires to produce cooling at low temperatures.

Returning to the usefulness of thermoelectric measurements as a characterization tool, data with very similar features to those of the double quantum dot data presented in Paper VI will now be discussed. The data were obtained from a long InAsP quantum dot defined in an InAs nanowire by two InP barriers. The thermocurrent behaves fairly normally for $V_H = 12$ mV (as shown in Figure 8.3 (c)), with the expected oscillatory lineshape for each conductance peak (as shown in Figure 8.3 (a)), separated by approximately 9 mV in V_g. As the heating voltage is increased, overall oscillatory behavior of the thermocurrent becomes apparent on a larger scale ($\Delta V_g = 200$ mV), resulting in regions with a completely positive or negative signal (as shown in Figure 8.3 (c)), which is not expected for a normal quantum dot. This thermoelectric behavior, which is very similar to that presented in Paper VI, indicates that the intended single quantum dot has broken up into two; resulting in a double quantum dot. This interpretation is strengthened by closer inspection of the conductance measurements in Figure 8.3 (a), which show Coulomb blockade peaks with a small spacing of 9 mV in V_g, as well as oscillation in the magnitude of the conductance peaks, with a period of approximately 200 mV. Some peaks also have opposite trends in amplitudes when the temperature of the measurement is increased, just as the data presented in Paper VI. Coulomb blockade spectroscopy also reveals very similar

74
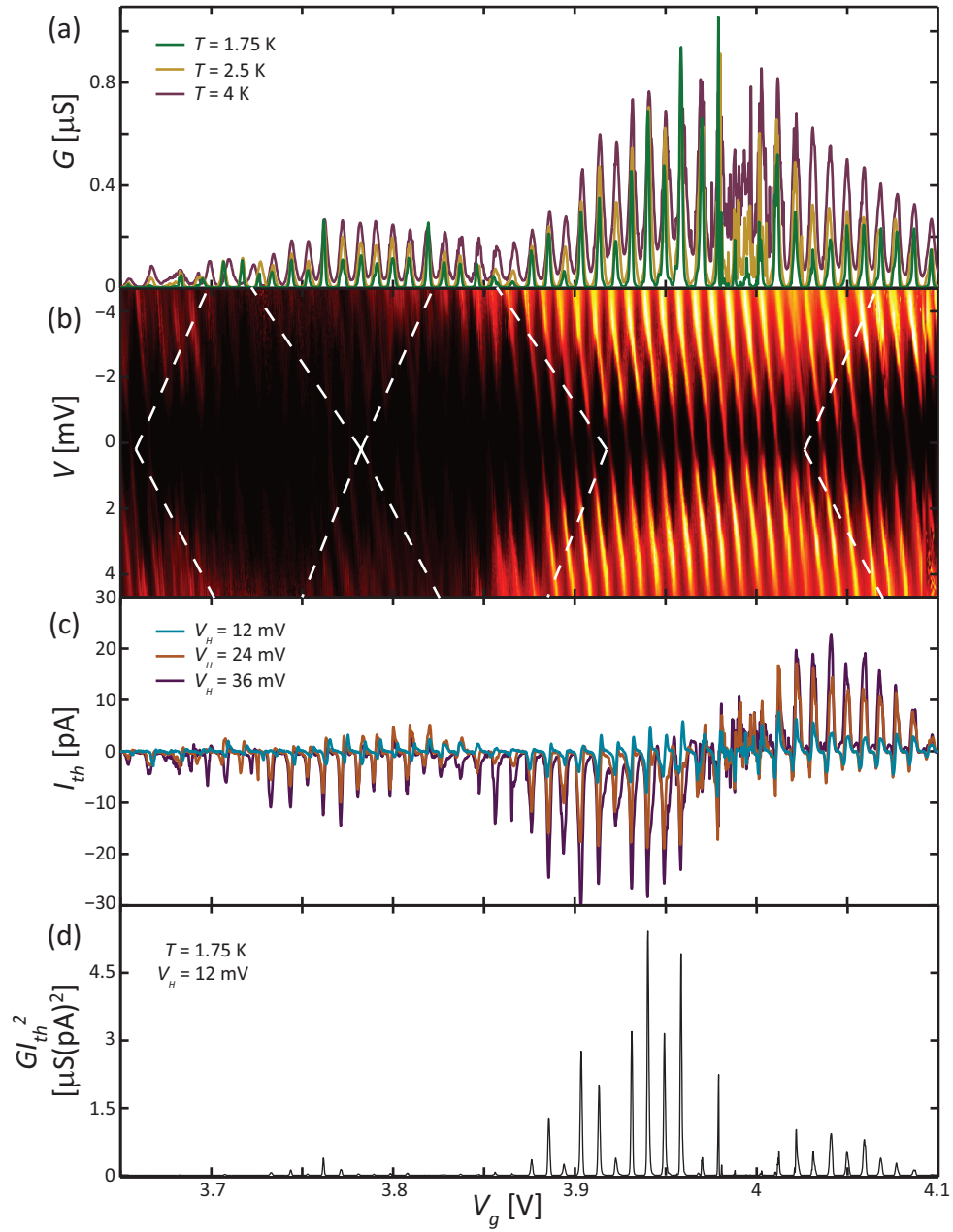
Figure 8.3. (a) Conductance, G, as a function of back-gate voltage, V_g, for three different temperatures, T. (b) Coulomb blockade spectroscopy in the same V_g region as in (a). The dashed white lines indicate the diamond-like pattern which is superimposed on the smaller diamond pattern caused by the Coulomb blockade peaks in (a). (c) Thermocurrent, I_{th}, as a function of V_g for three different heating voltages, V_H. (d) GI_{th}^2 as a function of V_g, calculated from the traces shown in (a) and (c). The data presented in this figure were obtained from an InAsP quantum dot defined in an InAs nanowire by InP barriers.

results to those presented in Paper VI. The pattern of Coulomb blockade diamonds consists of small diamonds overlaid by a pattern of larger diamond-like features, indicated by the white dashed lines in Figure 8.3 (b).

These results indicate the usefulness of thermoelectric measurements when characterizing a quantum dot. It is significantly easier to sweep the back-gate voltage at different heating voltages while measuring the thermovoltage or thermocurrent, than performing conductance measurements at different temperatures, which may be rather time consuming depending on the cryogenic system used. It is also quicker than a complete Coulomb blockade spectroscopy measurement, which usually requires quite some time to complete.

9. Conclusions and future work

Thermoelectric measurements can be performed for different purposes. Traditionally, they have been used to find ways of improving the efficiency of thermoelectric materials. However, during the past twenty years it has been shown that thermoelectric measurements can complement the more commonly used conductance measurements when characterizing a system. The thermoelectric response can, for example, be used to confirm an observation of a physical phenomenon seen in conductance, thereby making the measured data more credible. Thermoelectric measurements can also offer complementary information that cannot be obtained from conductance measurements, and may constitute a more accurate and straightforward characterization tool than conductance measurements.

Regardless of the purpose of the measurements, a good understanding of the thermoelectric response of a simple quantum dot provides a good foundation. The work presented in this thesis takes the first steps in this direction by thoroughly investigating the thermoelectric response of a quantum dot defined in a nanowire, with respect to its lineshape and nonlinear behavior. To do this, heterostructure nanowires must be grown (preferably straight and perpendicular to the substrate surface), and devices fabricated. Steps must also be taken to induce a temperature gradient along the length of the nanowire without disturbing its surroundings too much when designing thermoelectric devices.

Once an understanding of how a quantum dot responds to a temperature gradient has been obtained, it is possible to apply this knowledge to other more complicated systems. Unknown structures can be characterized and understood by combining thermoelectric measurements with conductance measurements; two such attempts have been presented in this thesis. Such measurements may even lead to discoveries of features that could improve thermoelectric efficiency. This approach to thermoelectricity is definitely not the most common, but could be valuable in that it tackles an old problem from a new perspective.

As indicated above, the work presented in this thesis has only scratched the surface, and much remains to be done. Some examples of interesting and unsolved problems are given below.

- Thermometry: if thermoelectric measurements are to be accepted as a characterization tool for nanostructured devices, a simple and straightforward way of measuring temperatures on the micrometer scale at low temperatures must be developed without the need for overly complicated device fabrication.

- Non-linear effects: The question of whether the nonlinear behavior we observed is the result of an increase in ΔT or in T remains to be answered. It will hopefully be simpler to investigate this with the new heating method proposed in Paper II, as the technique makes it possible to apply large temperature gradients without increasing the surrounding temperature. Knowledge on the relationship between nonlinear effects and energy level renormalization could be used to study such behavior in quantum dots.

- Quantum dot-like states: power factor enhancement was seen for InAs nanowires at low temperatures, and was attributed to quantum dot-like states. To fully understand this phenomenon it would be useful to be able to control it, and learn how to make use of it also at higher temperatures. It was originally proposed theoretically that this behavior was the result of modulations in the diameter of the nanowire. It is possible to induce such diameter modulations by, for example, etching selected parts of a nanowire. Another way to control quantum dot-like states would be to deliberately create them during growth. This could be done either by combining different materials (such as InAs and InAsP) or different crystal structures of the same material (wurtzite and zinc blende InAs, for example). The growth of both of these is feasible today [107, 108].

- Polymer electrolyte-gated nanowires: quantum dot-like states seem to be efficient for thermoelectric cooling at low temperatures, but the nanowires must be gated into their most efficient regions. A polymer electrolyte appears to provide a good alternative. Experiments should be carried out with the ultimate goal of embedding an entire array of nanowires, both n-type and p-type, in a polymer to make a complete thermoelectric element.

- Unintended double quantum dots: by fixing the charge environment of a nanowire with the aid of a polymer electrolyte gate, or the fabrication of long quantum dots can result in double quantum dot behavior. Efforts should be made to try to understand why this occurs, perhaps by intentionally creating such a weakly formed structure during growth. This could help us gain an understanding of the reason for the formation of quantum dot-like states in some nanowires.

- Characterization: many physical phenomena in nanostructures have been studied with conductance measurements during the past thirty years. The question now is, what new information can be obtained from the thermoelectric response. Some phenomena are more appealing than others, such as the valley of conductance suppression where conductance is vanishingly small [109], while the thermoelectric response may not be. Another example is to experimentally confirm the theoretically predicted possibility of using thermopower to detect the onset of Wigner localization of electrons in nanowire segments [81]. This is a new and exciting field of physics where there is considerable scope for future studies.

Appendix A – Preparation of chips for contacting nanowires

A highly doped 2-inch Si wafer is needed to make the pre-patterning on the chips used for making devices. The wafer is thermally oxidized to obtain a layer of SiO_2 around 100 nm thick. A layer of resist (S-1813) is then spun onto the front to protect the oxide layer on that side of the wafer. The wafer is then placed in an oxygen plasma ashing system for 2 minutes without cage with the reverse side facing up to make sure there is no resist left on this side of the wafer. The wafer is then placed in buffered hydrofluoric acid (BHF). When all the oxide has been etched away from the reverse side, the surface becomes hydrophobic and the BHF forms droplets instead of a liquid film covering the entire wafer. The wafer is then rinsed in water before being placed in the evaporator for the evaporation of 5 nm Ti and 100 nm Au onto the reverse side. This metal layer will act as the back gate during future measurements.

To make the markers that aid in the process of locating the nanowires when contacting them, a new resist (ZEP) is spun onto the front of the wafer. A pattern of small dots is thereafter created on the wafer using electron beam lithography. The pattern is developed, and the wafer is placed in the oxygen plasma ashing system for 45 seconds with cage. A 3 nm layer of Ti and a 30 nm layer of Au are then evaporated onto the wafer and lift-off is performed in S-1165. The sample is then cleaned in an ultrasonic bath, first in acetone, then in isopropyl alcohol (IPA).

The final step is the creation of bond pads. This is done using ultraviolet lithography (UVL). UVL is performed using a double layer of photoresist. First a layer of LOR 7B is spun onto the front of the wafer which is baked in an oven for 20 minutes at 180 °C. Then, a layer of S-1813 is spun on top of this and the wafer is baked on a hotplate for 90 seconds at 115 °C. The pattern is thereafter created in the UVL system, and developed in MF-319 for 30 seconds. The wafer is then placed in the oxygen plasma ashing system (45 seconds with cage) and layers of Ti (5 nm) and Au (100 nm) are thereafter evaporated onto the wafer. Lift-off is performed in S-1165, and the wafer is then cleaned in the ultrasonic bath, with first acetone and then IPA.

The wafer now has the required pattern, and is cut into small pieces that can be used for nanowire contacting. Such a piece, or chip, is shown in Figure 4.1 (a).

Appendix B – Details of device fabrication

The chip with deposited nanowires is prepared for electron beam lithography (EBL) by spinning 5% polymethyl methacrylate (PMMA) in anisole onto it at 5000 rpm for 1 minute. After spin-coating, the sample is baked on a hotplate at 180 °C for 3 minutes. It is thereafter transferred to the EBL unit for patterning. PMMA is a positive resist, and the chemical structure of the exposed region can be changed by de-cross-linking during exposure, making it soluble in a developer. After exposure in the EBL unit, the sample is developed in a 1:3 mixture of methyl isobutyl ketone and isopropyl alcohol (IPA) for 30 seconds, followed by a 30-second rinse in IPA. The pattern developed in the resist is thus identical to the pattern written by the electron beam. The sample is then placed in an oxygen plasma ashing system for 30 seconds at an oxygen pressure of 5 mbar to remove the last traces of resist from the exposed surface areas. Sulfur passivation is performed in a 1:9 (NH4)2Sx:H2O solution immediately before the sample is loaded into a Pfeiffer Classic 500 thermal evaporator where the 5 nm of either Ni or Ti followed by 75 nm Au is deposited. After evaporation the entire chip is covered with the metal stack. Lift-off is performed to remove the excess material, and to do this the sample is placed in a beaker of acetone on a hotplate at 80 °C for 15 minutes.

Acknowledgements

Thank you, Heiner! I don't know, and will probably never understand, why you contacted me and asked if I was interested in the PhD position in thermoelectrics that you had announced. I am very grateful that you did though! We have had some bumps on our journey to get here, but I have enjoyed almost every single day. I very much appreciate that I got the opportunity to work with you; you have a passion for research and a way to inspire people that I admire.

I also want to thank my assistant supervisors; Kimberly, Claes & Lars. I, especially, want to thank Kimberly for our hour-long discussions about science, research and life in general. And Claes, thank you for always being available for my questions, both big and small. And thank you for my word, you are, and will most likely remain, the only person who has ever given me a word. And just so you know, "Allt bra?" will forever be my favorite question just because of you!

My own fairy assistant supervisor, Adam Micolich! I don't know if you ever will realize how much you did for me when you let me come visit you and your group at UNSW in Sydney. Those three months gave me at least as much as the five years I have spent here in Lund in so many ways. Thank you!

When mentioning Sydney and UNSW I also want to thank all the really nice people that I got to know during my stay there, you all made me feel so incredibly welcome. I especially want to thank Sarah for becoming my pen pal, you are probably the only person in the world who I am certain understands how I have felt during these years as a PhD student. And Daisy, thank you for being the funniest lab buddy I have ever had. I will never forget those yucky eggs, and our hours practicing how to say r… Last, but definitely not least, Adam Burke! Without you I don't think I would have enjoyed my time at UNSW even half as much. You made me a better researcher, and a better person, thank you! And thank you for reading my thesis, and adding an incredible amount of commas!

I have been lucky enough to be part of a few publications, and all the work therein is certainly not solely mine. I would, therefore, like to take the opportunity to thank the other gifted researchers I have gotten the opportunity to work with: Ann, Eric, Natt, Henrik, Hongqi, Phil, Johannes, Sören, Jan-Göran, Xanthi, Kornelius, David, Slava, Damon & Martin L. A special thanks to you, Xanthi, for all the fun we had together

when we met at conferences. And one to Martin L for taking the time to explain weird theoretical stuff to me, and for commenting on my thesis.

I also want to thank all my present and former colleagues at the Division of Solid State Physics here in Lund. We all together make this a great place to do science, but also a fun place to spend a large part of our lives! Some people deserve an extra thank you for all their hard work. What would we do (or have done) without our wonderful ladies: Mona, Monica, Mari, Line, Margareta, Eva, Gerda, Lena, Anneli, Elsie & Karin. And our ever so handsome gentlemen: Håkan, George, Mariusz, Anders K, Sören, Bengt M, Peter B, Peter R, Ivan M, Nicklas, Bengt B, Janne, Johan & Thord. Thank you all so very much for keeping this division real, and functional!

A special thank you to Leif, for keeping us supplied with liquid nitrogen and helium. The work you do makes the life as a low-temperature researcher so much easier, and that you do it with a smile is worth more to me than anything, thank you!

Kilian, you have been the best office mate I could ever have wished for. Your patience and support has been what has gotten me through many days at work. Thank you for turning our office into a jungle, it made every day a better day!

The she-wolf pack - Sofia, Sepideh, Mercy, Karla, Linda, Susanne & Maria, you have kept me happy and smiling during these five years. Whenever I needed someone to talk to, laugh with, complain to or simply just vent with I could always turn to you. Thank you for that! We have also had an enormous amount of fun together, especially during our trips. I really hope that there will be more of those in the future!

Charlotta, you became my mentor by chance, and then we became friends. You always have time for a lunch when I need it, and your guidance is very much appreciated. You remind me of what is real, and what is not, and that has been very important for me, thank you!

Mats-Erik, meeting you is like a great adventure, every time! Thank you for introducing me to the world of honey badgers and bit coins. The chocolate is always delicious by the way! I should also thank Jonas J, Anders K, Line, Kilian & Maria for supporting Mats-Erik in the rather exhausting task of keeping me supplied with chocolate.

I have had the privilege to get to know a bunch of people in other divisions, departments, and even other faculties, and I want to thank you all for being a part of my life. I especially want to mention my friends in Mathematical Physics, Nuclear Physics and at EIT. The Voice-group also deserves a thank you, who would have known that taking one course could give so much perspective on life, and result in so many nice after-work dinners.

Another group of people that deserve a big thank you are all the PhD students who put in time and energy into the Doctoral section at LTH. I have had a lot of fun working with you, and even though everything is slow I am certain that we improve things a little every single day.

A warm thank you to the people who made all the crazy activities organized within Fun in Fysicum possible: Elin, Maciek, Daniel, Kilian, Maria, David, Cassie, Francesc & Holger. Unfortunately it turns out that Fysicum is the place where fun comes to die, but for a couple of years we stood up pretty well against the unavoidable…

Hanna, Ulrika, Ylva, Johanna, Karolina, Dan & Daniel, tjejerna som började Yi 2004 är verkligen inte som andra killar! Ett speciellt tack vill jag rikta till Johanna för att hon stod ut med en 19-åring det där första året i Linköping... Ulrika, tack för att du stod ut med ganska mycket gnällande angående en viss persons doktorerande! Och Hanna, du är storasystern jag aldrig hade!

Mamma & pappa, tack för ert helhjärtade stöd i allt jag gjort sedan jag föddes! Tack för att ni alltid har utmanat mig att bli bättre, både som person och i mina studier. Ni är fantastiska föräldrar och ni borde vara stolta över er själva och det utmärkta arbete ni gjort, och fortfarande gör, som sådana. Jag är stolt över att kunna säga att ni är min mamma och pappa, och jag älskar er, för evigt och alltid! Jag vill också tacka för de tre syskon jag fick av er, utan er och dem skulle jag inte vara den jag är.

Andreas, Malin & Beata, jag har känt er i hela era liv! Vi har gjort mycket roligt ihop redan och jag ser fram emot en massa fler år med oändligt många kul hittepå tillsammans med er. Det kanske inte fanns tid för Bejjan-dagen i år, men nästa år kommer den att återkomma och göra större succé än någonsin! Jag vill också passa på att tacka John för att du finns i Malins liv och att du tog dig tid och läste och kommenterade den här avhandlingen!

Mormor & morfar, jag vet att ni sitter någonstans där uppe och håller ett vakande öga på oss som är kvar här nere. Och äntligen är ni tillsammans igen!

Farmor & farfar, att höra er säga att ni är stolta över mig, och att ni skryter med vad jag har åstadkommit, gör det värt varenda uns av slit jag lagt ner för att ta mig dit jag är idag.

Tony, Billy, Alikos, Sonja, Gangster & Morris, jag har för alltid gett en liten bit av mitt hjärta till var och en av er. Ni var under en lång tid mina bästa vänner! Och Tony, du förblir den finaste (och knasigaste) av hästar i världen!

Helen, Lennart, Sofie, Thomas, Henrik & Fanny, tack för att ni är en så fantastisk familj! Från första gången jag träffade er och alla gånger efter det så har jag alltid känt

mig välkommen och uppskattad av er alla, och det är en underbar känsla. Den värme och glädje ni besitter önskar jag att fler människor kunde få uppleva!

Allra mest vill jag tacka Martin! Tack för att du så tålmodigt har stått ut med mig under de här snart fem åren jag har doktorerat. Ibland har livet lekt, och mitt doktorerande har gjort att vi fått uppleva underbara saker tillsammans. Ibland har allt bara varit en enda stor katastrof, och många gånger har det tyvärr gått ut över dig. En sak vet jag med säkerhet, utan dig hade jag aldrig orkat! Jag älskar dig!

<div style="text-align: right">

Sofia Fahlvik Svensson
Lund, 2014-09-08

</div>

References

[1]   Ioffe A F, Stilbans L S, Iordanishvili E K, Stavitskaya T S, Gelbtuch A and Vineyard G, *Physics Today* **12**, 42 (1959)

[2]   Mahan G, Sales B and Sharp J, *Physics Today* **50**, 42 (1997)

[3]   Jonson M and Mahan G D, *Physical Review B* **21**, 4223 (1980)

[4]   Dresselhaus M S, Chen G, Tang M Y, Yang R G, Lee H, Wang D Z, Ren Z F, Fleurial J P and Gogna P, *Advanced Materials* **19**, 1043 (2007)

[5]   Cornett J E and Rabin O, *Physical Review B* **84**, 205410 (2011)

[6]   Cahill D G, Ford W K, Goodson K E, Mahan G D, Majumdar A, Maris H J, Merlin R and Sr P, *Journal of Applied Physics* **93**, 793 (2003)

[7]   Hicks L D and Dresselhaus M S, *Physical Review B* **47**, 16631 (1993)

[8]   Hicks L D and Dresselhaus M S, *Physical Review B* **47**, 12727 (1993)

[9]   Mahan G D and Sofo J O, *Proceedings of the National Academy of Sciences of the United States of America* **93**, 7436 (1996)

[10]   Humphrey T E, Newbury R, Taylor R P and Linke H, *Physical Review Letters* **89**, 116801 (2002)

[11]   Seebeck T J, *Annalen der Physik und Chemie* **6**, 1 (1826)

[12]   Peltier J C A, *Annales de Chimie et de Physique* **56**, 371 (1834)

[13]   O'Dwyer M F, Humphrey T E and Linke H, *Nanotechnology* **17**, S338 (2006)

[14]   Staring A A M, Molenkamp L W, Alphenaar B W, van Houten H, Buyk O J A, Mabesoone M A A, Beenakker C W J and Foxon C T, *Europhysics Letters* **22**, 57 (1993)

[15]   Fowler A B, Fang F F, Howard W E and Stiles P J, *Physical Review Letters* **16**, 901 (1966)

[16]   Stern F and Howard W E, *Physical Review* **163**, 816 (1967)

[17]   Björk M T, Ohlsson B J, Sass T, Persson A I, Thelander C, Magnusson M H, Deppert K, Wallenberg L R and Samuelson L, *Nano Letters* **2**, 87 (2002)

[18]   Nilsson H A, Deng M T, Caroff P, Thelander C, Samuelson L, Wernersson L E and Xu H Q, *IEEE Journal of Selected Topics in Quantum Electronics* **17**, 907 (2011)

[19]   Yazawa M, Koguchi M, Muto A, Ozawa M and Hiruma K, *Applied Physics Letters* **61**, 2051 (1992)

[20]   Ohlsson B J, Björk M T, Magnusson M H, Deppert K, Samuelson L and Wallenberg L R, *Applied Physics Letters* **79**, 3335 (2001)

[21]   van Wees B J, van Houten H, Beenakker C W J, Williamson J G, Kouwenhoven L P, van der Marel D and Foxon C T, *Physical Review Letters* **60**, 848 (1988)

[22]   Wharam D A, Thornton T J, Newbury R, Pepper M, Ahmed H, Frost J E F, Hasko D G, Peacock D C, Ritchie D A and Jones G A C, *Journal of Physics C-Solid State Physics* **21**, L209 (1988)

[23]   Björk M T, Ohlsson B J, Thelander C, Persson A I, Deppert K, Wallenberg L R and Samuelson L, *Applied Physics Letters* **81**, 4458 (2002)

[24]   Stringfellow G B *Organometallic Vapor-Phase Epitaxy : Theory and Practice* (San Diego, Academic Press, 1999)

[25]   Mårtensson T, Borgström M, Seifert W, Ohlsson B J and Samuelson L, *Nanotechnology* **14**, 1255 (2003)

[26]   Biasiol G, Sorba, L. *Molecular beam epitaxy: principles and applications, in Crystal growth of materials for energy production and energy* (Pisa, Edizioni ETS, 2001) pp 66-83

[27]   Panish M B and Temkin H *Gas Source Molecular Beam Epitaxy* (Berlin, Springer-Verlag, 1993)

[28]   Ritter D and Heinecke H, *Journal of Crystal Growth* **170**, 149 (1997)

[29]   Jensen L E, Björk M T, Jeppesen S, Persson A I, Ohlsson B J and Samuelson L, *Nano Letters* **4**, 1961 (2004)

[30]   Persson A I, Fröberg L E, Jeppesen S, Björk M T and Samuelson L, *Journal of Applied Physics* **101**, 034313 (2007)

[31]   Thelander C, Björk M T, Larsson M W, Hansen A E, Wallenberg L R and Samuelson L, *Solid State Communications* **131**, 573 (2004)

[32]   Tsui D C, *Physical Review Letters* **24**, 303 (1970)

[33]   Larsson M W, Wagner J B, Wallin M, Håkansson P, Fröberg L E, Samuelson L and Wallenberg L R, *Nanotechnology* **18**, 015504 (2007)

[34]   Hiruma K, Murakoshi H, Yazawa M and Katsuyama T, *Journal of Crystal Growth* **163**, 226 (1996)

[35]   Verheijen M A, Immink G, de Smet T, Borgström M T and Bakkers E P A M, *Journal of the American Chemical Society* **128**, 1353 (2006)

[36]   Clark T E, Nimmatoori P, Lew K K, Pan L, Redwing J M and Dickey E C, *Nano Letters* **8**, 1246 (2008)

[37]   Dick K A, Kodambaka S, Reuter M C, Deppert K, Samuelson L, Seifert W, Wallenberg L R and Ross F M, *Nano Letters* **7**, 1817 (2007)

[38]   Paladugu M, Zou J, Guo Y N, Auchterlonie G J, Joyce H J, Gao Q, Tan H H, Jagadish C and Kim Y, *Small* **3**, 1873 (2007)

[39]   Messing M E, Wong-Leung J, Zanolli Z, Joyce H J, Tan H H, Gao Q, Wallenberg L R, Johansson J and Jagadish C, *Nano Letters* **11**, 3899 (2011)

[40]   Suyatin D B, Thelander C, Björk M T, Maximov I and Samuelson L, *Nanotechnology* **18**, 105307 (2007)

[41]   Petrovykh D Y, Yang M J and Whitman L J, *Surface Science* **523**, 231 (2003)

[42]   Hoffmann E A, *The thermoelectric efficiency of quantum dots in InAs/InP nanowires*, PhD thesis, University of Oregon (2009)

[43]   Hoffmann E A, Nilsson H A, Matthews J E, Nakpathomkun N, Persson A I, Samuelson L and Linke H, *Nano Letters* **9**, 779 (2009)

[44]   Tian Y, Sakr M R, Kinder J M, Liang D, MacDonald M J, Qiu R L J, Gao H J and Gao X P A, *Nano Letters* **12**, 6492 (2012)

[45]   Moon J, Kim J H, Chen Z C Y, Xiang J and Chen R K, *Nano Letters* **13**, 1196 (2013)

[46]   Mitdank R, Handwerg M, Steinweg C, Tollner W, Daub M, Nielsch K and Fischer S F, *Journal of Applied Physics* **111**, 104320 (2012)

[47]   Pobell F *Matter and Methods at Low Temperatures* (Berlin, Springer-Verlag, 2007)

[48]   de Waele A T A M, *Journal of Low Temperature Physics* **164**, 179 (2011)

[49]   Scofield J H, *American Journal of Physics* **62**, 129 (1994)

[50]   Hoffmann E A, Nilsson H A, Samuelson L and Linke H, *AIP Conference Proceedings* **397,** 1399 (2011)

[51]   Hoffmann E A and Linke H, *Journal of Low Temperature Physics* **154**, 161 (2009)

[52]   Nakpathomkun N, *Thermoelectric properties of quantum dots and other low-dimensional systems*, PhD thesis, University of Oregon (2010)

[53]   Hoffmann E A, Nakpathomkun N, Persson A I, Linke H, Nilsson H A and Samuelson L, *Applied Physics Letters* **91**, 252114 (2007)

[54]   Hoffmann E A, Nakpathomkun N, Persson A I, Nilsson H A, Samuelson L and Linke H, *Physica E-Low-Dimensional Systems & Nanostructures* **40**, 1605 (2008)

[55]   Weis J, in *CFN Lectures on Functional Nanostructures Vol. 1*, edited by K. Busch, A. Powell, C. Röthig, G. Schön and J. Weissmüller (Berlin, Springer-Verlag, 2005), Vol. 658, pp. 87.

[56]   Meirav U, Kastner M A and Wind S J, *Physical Review Letters* **65**, 771 (1990)

[57]   Heinzel T *Mesoscopic Electronics in Solid State Nanostructures* (Weinheim, WILEY-VCH Verlag GmbH & Co., 2007)

[58]   Kouwenhoven L P, Austing D G and Tarucha S, *Reports on Progress in Physics* **64**, 701 (2001)

[59]   De Franceschi S, Sasaki S, Elzerman J M, van der Wiel W G, Tarucha S and Kouwenhoven L P, *Physical Review Letters* **86**, 878 (2001)

[60]   Averin D V and Nazarov Y V, *Physical Review Letters* **65**, 2446 (1990)

[61]   Küng B, Rössler C, Beck M, Faist J, Ihn T and Ensslin K, *New Journal of Physics* **14**, 083003 (2012)

[62]   König J, Schoeller H and Schön G, *Europhysics Letters* **31**, 31 (1995)

[63]   Joyez P, Bouchiat V, Esteve D, Urbina C and Devoret M H, *Physical Review Letters* **79**, 1349 (1997)

[64]   Datta S *Electronic Transport in Mesoscopic Systems* (Cambridge, Cambridge University Press, 1995)

[65]   Dubi Y and Di Ventra M, *Reviews of Modern Physics* **83**, 131 (2011)

[66]   Mani P, Nakpathomkun N, Hoffmann E A and Linke H, *Nano Letters* **11**, 4679 (2011)

[67]   Beenakker C W J and Staring A A M, *Physical Review B* **46**, 9667 (1992)

[68]   Dzurak A S, Smith C G, Pepper M, Ritchie D A, Frost J E F, Jones G A C and Hasko D G, *Solid State Communications* **87**, 1145 (1993)

[69]   Cutler M and Mott N F, *Physical Review* **181**, 1336 (1969)

[70] Dzurak A S, Smith C G, Barnes C H W, Pepper M, Martin-Moreno L, Liang C T, Ritchie D A and Jones G A C, *Physical Review B* **55**, 10197 (1997)

[71] Turek M and Matveev K A, *Physical Review B* **65**, 115332 (2002)

[72] Scheibner R, Novik E G, Borzenko T, König M, Reuter D, Wieck A D, Buhmann H and Molenkamp L W, *Physical Review B* **75**, 041301 (2007)

[73] Pogosov A G, Budantsev M V, Lavrov R A, Plotnikov A E, Bakarov A K, Toropov A I and Portal J C, *JETP Letters* **83**, 122 (2006)

[74] Sierra M A and Sánchez D, http://arxiv.org/abs/1408.0181 (2014)

[75] Humphrey T E and Linke H, *Physical Review Letters* **94**, 096601 (2005)

[76] Majumdar A, *Science* **303**, 777 (2004)

[77] Turek M, Siewert J and Richter K, *Physical Review B* **71**, 220503(R) (2005)

[78] Sivan U and Imry Y, *Physical Review B* **33**, 551 (1986)

[79] Schmidt V, Mensch P F J, Karg S F, Gotsmann B, Das Kanungo P, Schmid H and Riel H, *Applied Physics Letters* **104**, 012113 (2014)

[80] Dzurak A S, Smith C G, Barnes C H W, Pepper M, Martin-Moreno L, Liang C T, Ritchie D A and Jones G A C, *Physica B* **251**, 281 (1998)

[81] Kristinsdóttir L H, Bengtsson J, Linke H, Reimann S M and Wacker A, *Applied Physics Letters* **105**, 083105 (2014)

[82] Möller S, Buhmann H, Godijn S F and Molenkamp L W, *Physical Review Letters* **81**, 5197 (1998)

[83] Buhmann H, Möller S, Godijn S F and Molenkamp L W, *Physica B-Condensed Matter* **256**, 198 (1998)

[84] Godijn S F, Möller S, Buhmann H, Molenkamp L W and van Langen S A, *Physical Review Letters* **82**, 2927 (1999)

[85] Scheibner R, Buhmann H, Reuter D, Kiselev M N and Molenkamp L W, *Physical Review Letters* **95**, 176602 (2005)

[86] Seol J H, Moore A L, Saha S K, Zhou F, Shi L, Ye Q L, Scheffler R, Mingo N and Yamada T, *Journal of Applied Physics* **101**, 023706 (2007)

[87] Roddaro S, Ercolani D, Safeen M A, Suomalainen S, Rossella F, Giazotto F, Sorba L and Beltram F, *Nano Letters* **13**, 3638 (2013)

[88] van Weperen I, Plissard S R, Bakkers E P A M, Frolov S M and Kouwenhoven L P, *Nano Letters* **13**, 387 (2013)

[89] Streda P, *Journal of Physics-Condensed Matter* **1**, 1025 (1989)

[90] Molenkamp L W, van Houten H, Beenakker C W J, Eppenga R and Foxon C T, *Physical Review Letters* **65**, 1052 (1990)

[91] Dzurak A S, Smith C G, Martin-Moreno L, Pepper M, Ritchie D A, Jones G A C and Hasko D G, *Journal of Physics-Condensed Matter* **5**, 8055 (1993)

[92] Nakpathomkun N, Xu H Q and Linke H, *Physical Review B* **82**, 235428 (2010)

[93] Zianni X, *Applied Physics Letters* **97**, 233106 (2010)

[94] Zianni X, *Nanoscale Research Letters* **6**, 286 (2011)

[95] Lu W, Xie P and Lieber C M, *IEEE Transactions on Electron Devices* **55**, 2859 (2008)

[96] Cui Y, Duan X F, Hu J T and Lieber C M, *Journal of Physical Chemistry B* **104**, 5213 (2000)

[97] Duan X F, Huang Y, Cui Y, Wang J F and Lieber C M, *Nature* **409**, 66 (2001)

[98]   Fasth C, Fuhrer A, Björk M T and Samuelson L, *Nano Letters* **5**, 1487 (2005)

[99]   Pfund A, Shorubalko I, Leturcq R and Ensslin K, *Applied Physics Letters* **89**, 252106 (2006)

[100]   Bryllert T, Wernersson L E, Löwgren T and Samuelson L, *Nanotechnology* **17**, S227 (2006)

[101]   Dhara S, Sengupta S, Solanki H S, Maurya A, Pavan A, Gokhale M R, Bhattacharya A and Deshmukh M M, *Applied Physics Letters* **99**, 173101 (2011)

[102]   Storm K, Nylund G, Samuelson L and Micolich A P, *Nano Letters* **12**, 1 (2012)

[103]   Liang D and Gao X P A, *Nano Letters* **12**, 3263 (2012)

[104]   Carrad D J, Burke A M, Lyttleton R W, Joyce H J, Tan H H, Jagadish C, Storm K, Linke H, Samuelson L and Micolich A P, *Nano Letters* **14**, 94 (2014)

[105]   Kim S H, Hong K, Xie W, Lee K H, Zhang S P, Lodge T P and Frisbie C D, *Advanced Materials* **25**, 1822 (2013)

[106]   Panzer M J and Frisbie C D, *Advanced Functional Materials* **16**, 1051 (2006)

[107]   Persson A I, Björk M T, Jeppesen S, Wagner J B, Wallenberg L R and Samuelson L, *Nano Letters* **6**, 403 (2006)

[108]   Dick K A, Bolinsson J, Messing M E, Lehmann S, Johansson J and Caroff P, *Journal of Vacuum Science & Technology B* **29**, 04D103 (2011)

[109]   Nilsson H A, Karlström O, Larsson M, Caroff P, Pedersen J N, Samuelson L, Wacker A, Wernersson L E and Xu H Q, *Physical Review Letters* **104**, 186804 (2010)